# Proof of Concept

*wave energized baltic aeration pump (WEBAP)*

Margheritini, Lucia; Parmeggiani, Stefano; Kofoed, Jens Peter; Sumila, Arnas

*Publication date:*
2010

*Document Version*
Publisher's PDF, also known as Version of record

# Proof of concept: Wave Energized Baltic Aeration Pump (WEBAP)

**L. Margheritini**
**S. Parmeggiani**
**J. P. Kofoed**
**A. Sumila**

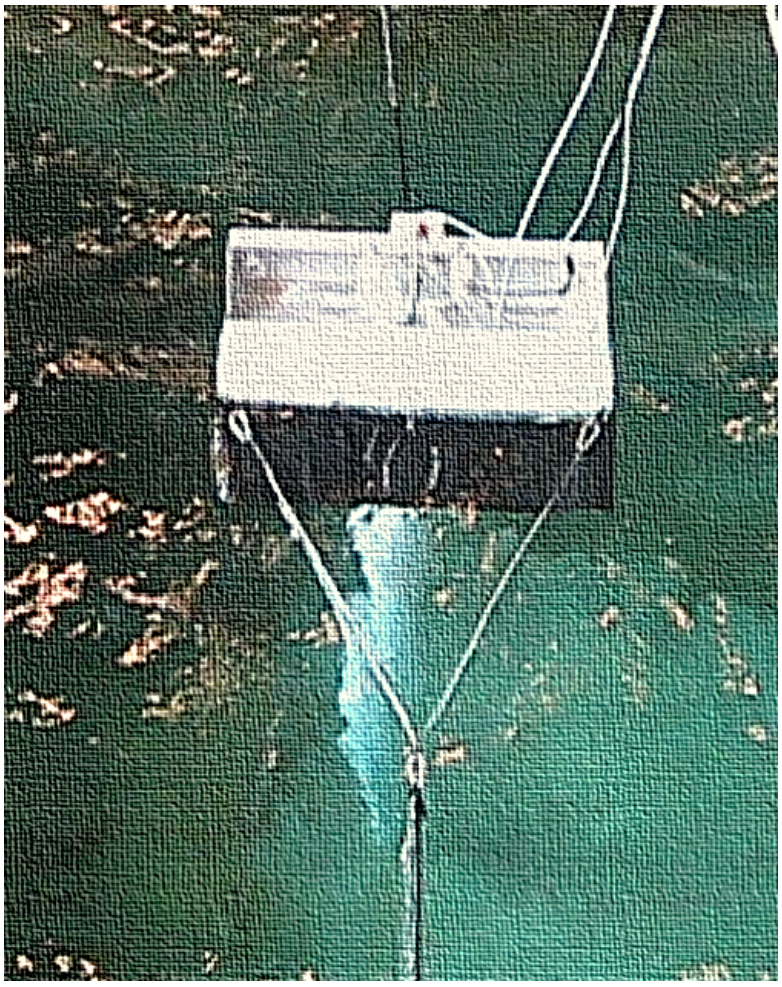

**ISSN 1901-726X**
**DCE Technical Report No. 82**

AALBORG UNIVERSITY
**Department of Civil Engineering**

Aalborg University
Department of Civil Engineering
Group Name

**DCE Technical Report No. 82**

# Proof of concept: Wave Energized Baltic Aeration Pump (WEBAP)

by

L. Margheritini
S. Parmeggiani
J. P. Kofoed
A. Sumila

November 2010

## Scientific Publications at the Department of Civil Engineering

***Technical Reports*** are published for timely dissemination of research results and scientific work carried out at the Department of Civil Engineering (DCE) at Aalborg University. This medium allows publication of more detailed explanations and results than typically allowed in scientific journals.

***Technical Memoranda*** are produced to enable the preliminary dissemination of scientific work by the personnel of the DCE where such release is deemed to be appropriate. Documents of this kind may be incomplete or temporary versions of papers—or part of continuing work. This should be kept in mind when references are given to publications of this kind.

***Contract Reports*** are produced to report scientific work carried out under contract. Publications of this kind contain confidential matter and are reserved for the sponsors and the DCE. Therefore, Contract Reports are generally not available for public circulation.

***Lecture Notes*** contain material produced by the lecturers at the DCE for educational purposes. This may be scientific notes, lecture books, example problems or manuals for laboratory work, or computer programs developed at the DCE.

***Theses*** are monograms or collections of papers published to report the scientific work carried out at the DCE to obtain a degree as either PhD or Doctor of Technology. The thesis is publicly available after the defence of the degree.

***Latest News*** is published to enable rapid communication of information about scientific work carried out at the DCE. This includes the status of research projects, developments in the laboratories, information about collaborative work and recent research results.

Published 2010 by
Aalborg University
Department of Civil Engineering
Sohngaardsholmsvej 57,
DK-9000 Aalborg, Denmark

Printed in Aalborg at Aalborg University

ISSN 1901-726X
DCE Technical Report No. 82

**ISSN 1901-726X**
**DCE Technical Report No. 82**

## Preface

The Wave Energized Baltic Aeration Pump (WEBAP) is a concept that proposes to find a solution to the low level of oxygenation of the Baltic Sea by bringing the surface sea water to the depth where the oxygen is needed. It proposes to do so by using the rich in oxygen overtopping water collected in a reservoir floating on the sea. The stored water, after overtopping the ramp leading to the reservoir, will be at a higher level than mean water level and therefore will have a potential energy. This potential energy is indeed used to pump down to the sea bed the oxygenated water right there where it is needed.

In the following paragraphs, the desk study on the WEBAP concept is presented in terms of overtopping flow rates for different configurations. Investigations on different drafts, slope angles and crest levels have been completed. Calculations on the pipe discharge have been made in order to define the driving head. The results obtained are then used to realized the model in scale 1:25 to be tested in the Hydraulic and Costal Engineering Laboratory at Aalborg University, Denmark.

The desk study and the laboratory setup have been presented as draft at the beginning of September 2010.

Laboratory tests in scale 1:25 have been concluded at the beginning of October 2010 and the final report delivered in November. Results present mooring forces, motion functions of the floating body, rotational speed of the propeller in the pum-pipe system. Results are presented in full scale. In addition, videos and pictures of the tests are included in electronic version. Lucia Margheritini (lm@civil.aau.dk) has been the main responsible for the testing, data analysis and results in the report. Arnas Sumila (asumil10@student.aau.dk) took care of the measuring equipment and calculations in Chapter 3. Stefano Parmeggiani (sp@civil.aau.dk) helped on laboratory setup and testing and Jens Peter Kofoed (jpk@civil.aau.dk) provided supervision and advice.

| Version | Date | Comment | Responsible |
|---|---|---|---|
| 0.0 Complete final report | 19.11.2010 | Draft version containing Chapters 1, 2 and 3 has been sent in to the developers the 2nd of September 2010. A Note on preliminary results on mooring forces has been sent in at the end of September 2010. | LM |
| 0.1 Complete final report | 29.11.2010 | Pipe equations added. Line thickness in figures changed to 1. Doc layout changed. | LM |
| 0.2 Final report | 10.12.2010 | Included - comments and corrections from Lennart Claeson | LM |

# Table of Contents


1 Objectives of the investigation ..... 3

2 Estimation of overtopping ..... 4

2.1 Influence of crest freeboard $R_c$, ..... 4

2.2 Influence of ramp extension ..... 5

2.3 Influence of the slope angle ..... 9

2.4 Conclusions ..... 10

3 Estimation of pipe capacity as function of water level in the reservoir ..... 12

3.1 Conclusions ..... 14

4 Laboratory testing and model ..... 15

4.1 Laboratory set up ..... 15

4.2 Measuring equipment ..... 17

4.3 Wave characteristics ..... 18

Useful relations between wave parameters are: ..... 18

4.4 Conclusions ..... 18

5 Results and analysis ..... 19

5.1 Generated waves and tested configurations ..... 19

5.2 Moorings characteristics ..... 21

5.3 Free oscillation tests ..... 23

5.4 Mooring forces ..... 25

5.5 Overtopping and functioning of the pump system ..... 27

5.6 Motion transfer function ..... 28

5.7 Conclusions ..... 32

6 Notes and suggestions ..... 33

Reference ..... 33

A - Appendix ..... 34

# 1 Objectives of the investigation

The Wave Energized Baltic Aeration Pump (WEBAP) is a concept that proposes to find a solution to the low level of oxygenation of the Baltic Sea by bringing the surface sea water to the depth where the oxygen is needed. It proposes to do so by using the rich in oxygen overtopping water collected in a reservoir floating on the sea. The stored water, after overtopping the ramp leading to the reservoir, will be at a higher level than mean water level and therefore will have a potential energy. This potential energy is indeed used to pump down to the sea bed the oxygenated water right there where it is needed.

Based on the design the developers suggested, investigations on the Wave Energized Baltic Aeration Pump (WEBAP) concept have been carried out. The purposes of the investigation are:

- Proof of concept.
- Estimation of overtopping with the focus on given everyday wave conditions.
- Estimation of motions of the floating body with focus on extreme wave conditions.
- Estimation of mooring forces with focus on extreme wave conditions.

The investigation is divided in:

1) desk study, aimed at defining the best geometries to be tested in the laboratory and predict the overtopping for different crest levels (Chapter 2 and 3);
2) laboratory testing, focused on the motion of the floating body and on mooring forces (Chapter 4 and 5).

All the Sub-chapters have their own conclusions and an overview on the findings of the present report is given in Chapter 6 closing the document.

## 2 Estimation of overtopping

The geometry, provided by the developer, consists of a floating reservoir with a lower sloped side and virtually no draft. The bottom of the reservoir has a hole (water outlet) where a long flexible pipe is rigidly connected.

The mean overtopping discharge for this structure is calculated with the formulae by Kofoed (2002):

$$\frac{q}{\lambda_m \lambda_\alpha \lambda_{dr} \lambda_s \sqrt{g H_s^3}} = 0.2e^{-2.6 \frac{R_c}{H_s \gamma_r \gamma_b \gamma_h \gamma_\beta} \frac{1}{}} \quad (1)$$

Where Hs is the significant wave high, Rc is the crest free board and g the gravity acceleration=9.81 m/s2. The λ factors take into account different geometrical parameters such as varying slope angle, draft extension (dr) and small dimensionless free board $R = \frac{R_c}{H_s}$ (definition sketch, Fig 1). The γ coefficients are reduction coefficients as defined by van der Meer and Janssen (1995).

By mean of the above equation, the influence of different parameters such as crest free board Rc, draft extension dr and slope angle α on the overtopping flow rates has been explained.

### *2.1 Influence of crest freeboard $R_c$,*

For a fixed geometry and a slope angle of 23°, different crest freeboards are obtained by changing the buoyancy level of the model, meaning that the sum Rc+dr is a constant = 1.25 m in full scale, so that when we increase the Rc (creast free board) we decrease dr (draft). Therefore, in the present calculations Rc and dr are not independent one from the other. Based on this assumption, the results the overtopping discharge has been calculated in four different wave conditions (Fig. 2).

Higher overtopping volumes correspond to smaller Rc, bigger dr and bigger waves. As it seems obvious, the overtopping increases when decreasing the Rc up to a maximum that depends on the wave height. The steepness of the curves in Fig. 2 is bigger than in the case where only Rc varies, i.e. when Rc varies independently from dr. This is because increasing the draft dr increases the overtopping volumes in a similar way as decreasing Rc increases overtopping volumes. Therefore in Fig. 2 two positive effects on the overtopping are plotted in the same curves.

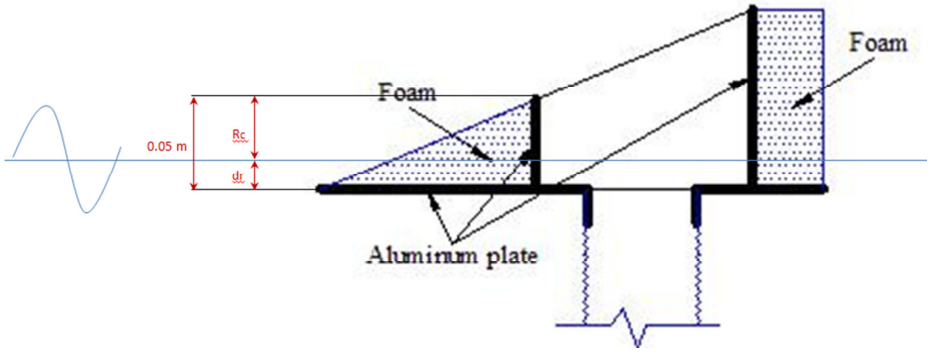


**Figure 1. Definition sketch, 1:25 to full scale, front slope angle = 23°.**

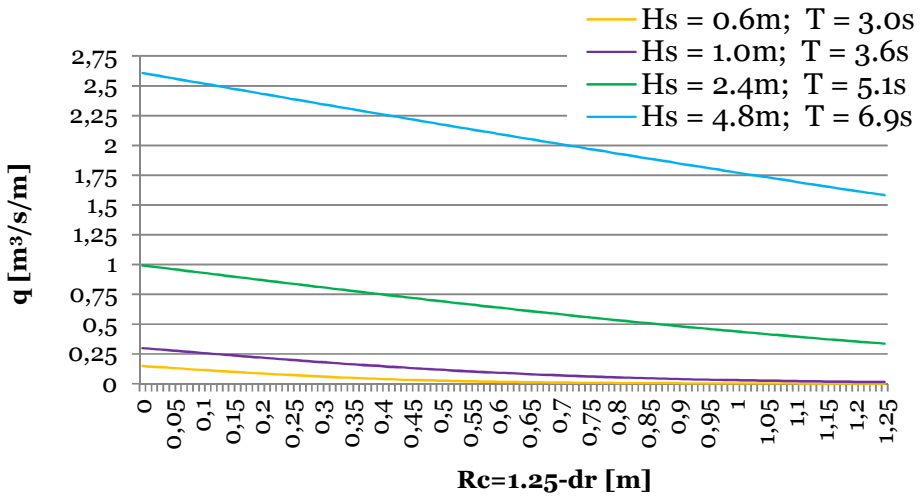


**Figure 2. Dependency of the overtopping discharge on the Rc and dr, for different wave conditions. Full scale values, geometry based on configuration in figure 1, slope angle =23°.**

## *2.2 Influence of ramp extension*

Extending the front ramp increases the draft of the floating body and the overtopping volumes by directing the flow that would pass under the device, to the reservoir. Based on this idea, the developer expressed the wish of adding a stretched cloth fixed on a steel frame to make the ramp longer and "capture" that flow. Despite the clothe not being the optimal solution to reach the purpose, calculations with three different "ramp extensions" have been made, in order to show what is possible to gain with such an implementation. The calculations, thought, are based on Equation (1) and therefore on one geometry where the ramp extension makes up one piece with the entire structure (Fig. 3). In the equation used to calculate the average overtopping discharge, the ramp extension is expressed by the coefficient $\lambda_{dr}$ and therefore by the draft:

$$\lambda_{dr} = 1 - k\frac{\sinh\left(2k_p d\left(1-\frac{d_r}{d}\right)\right)+2k_p d\left(1-\frac{d_r}{d}\right)}{\sinh(2k_p d)+2k_p d} \qquad (2)$$

where kp is the wave number based on Lp = wave length based on Tp and k is a coefficient controlling the degree of influence of the limited draft. k is found to be 0.4 by best fit to Kofoed (2002) tests; d is the water depth and the other parameters have been previously described. The expression taking the dependency of the draft into account is based on the ratio between the time averaged amount of energy flux integrated from the draft up to the surface Ef,dr and the time averaged amount of energy flux integrated from the seabed up to the surface Ef,d (Fig. 4):

$$\frac{E_{f,dr}}{E_{f,d}} = 1 - \frac{\sinh\left(2k_p d\left(1-\frac{d_r}{d}\right)\right)+2k_p d\left(1-\frac{d_r}{d}\right)}{\sinh(2k_p d)+2k_p d} \qquad (3)$$

In the derivation of Eq. 3 linear wave theory is used. Because of the limitations of the linear wave theory Eq. 3 cannot completely describe the effect of limited draft on overtopping. Using λdr equal to Eq. 3 would lead to an estimation of zero overtopping for dr=0 which obviously is not the case for all combinations of Hs and Rc. Therefore the coefficient k=0.4 is introduced and the expression for λdr given in Eq. 2 is obtained.

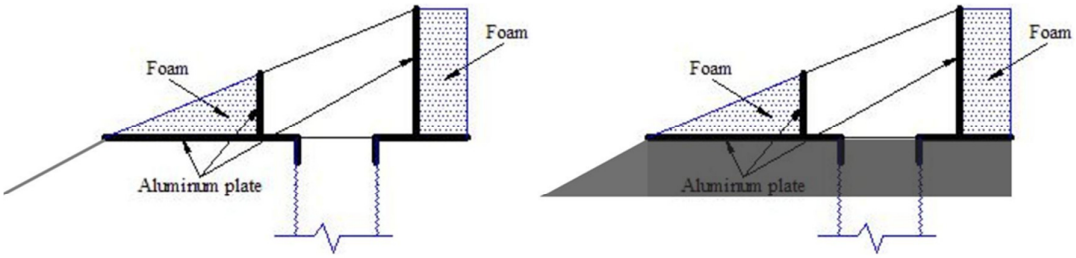


**Figure 3. The model whished by the developer (left) and the model used in the calculations, based on the hypothesis of Eq. 1 (right).**

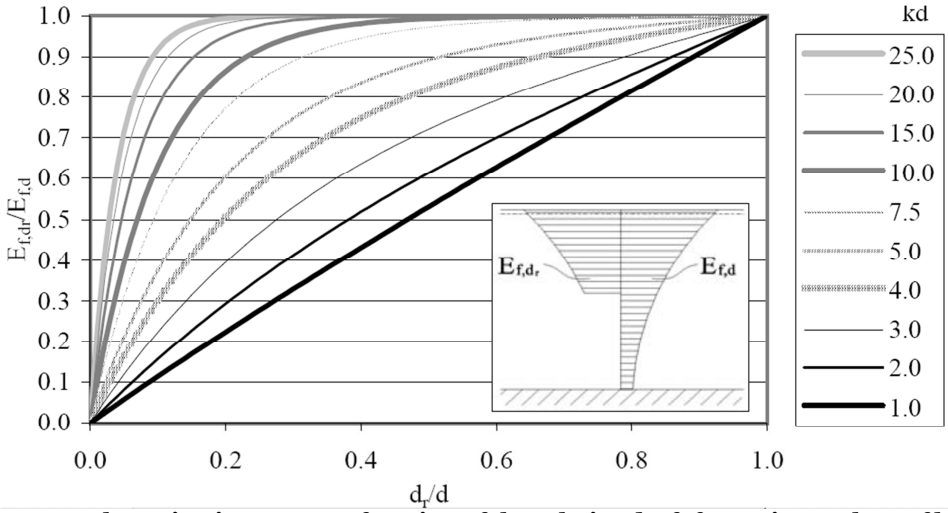


**Figure 4. The ration in Eq. 3 as a function of the relative draft for various values of kd.**

For the selected geometry with slope angle of 23˚, overtopping calculations have been made for a ramp extension of 2 m, 4 m and 6 m varying separately the draft dr and the crest level Rc that are not longer considered dependent on each others. However, if the WEBAP structure will be realized with a flexible slope, the results that follow must be decreased proportionally to the weakness of the material used. The losses depend on details that are not know at the present time of development of the device, such as the material of the extension, the connection to the main body, the inclination angle. It would be indeed expected that a flexible material without a rear support, would block and direct only a negligible flow to the reservoir, while most of it would pass under the structure. In addition such a solution may be not resistant and durable.

The extension of the ramp has positive effects on maximization of the overtopping volumes (Fig. 5-8).

In average, we foreseen an increase of overtopping volumes up to 16.5% for a ramp extension of 2 m compared with the case with no ramp extension for Hs = 0.6 m while for waves with Hs= 4.8 m the increase in overtopping is 6.9 %, with smaller variance compared to the case with smaller waves. This is because for smaller waves the overtopping is zero until the Rc is roughly 0.55 m and dr=0.70 m, being the waves too small to overtop the crest. Therefore an increase in the draft is more effective for lower sea states than in bigger waves as most of the incoming waves would overtop the crest anyways. With 2 m ramp extension, 0.020 m3/s/m of overtopping flow rates are reachable with Rc = 0.58 m while without the ramp the same results needs Rc = 0.55 m. If the

ramp extension is 6 m, then an average increase on the overtopping flow rate of 29% is expected for Hs = 0.6 m while an increase of 13% in the case with Hs=4.8 m.

For an Rc = 1.25 m (Table 1) and Hs = 0.6 m a ramp extension of 2 m with slope inclination of 23°, corresponding to a draft of 0.8 m, would generate an overtopping flow rate of 0.0010 m3/s/m; compared to the case with no draft that gives 0.0008 m3/s/m we have an increase of 33%. For Hs = 1.0 m passing from 2 m to 6 m a ramp extension would increase the overtopping flow rates from 0.0178 m3/s/m to 0.0214 m3/s/m corresponding to an increase of 25% and 51% respectively compared with the case with no draft that have an overtopping of 0.0142 m3/s/m. For Hs=2.4 m the increase in overtopping passing from the case with no ramp and the case with 6 m long ramp foreseen an increased in overtopping of 34% going from 0.3360 m3/s/m to 0.4503 m3/s/m while for Hs=4.8 m gives an increase of 21% with the longest extension.

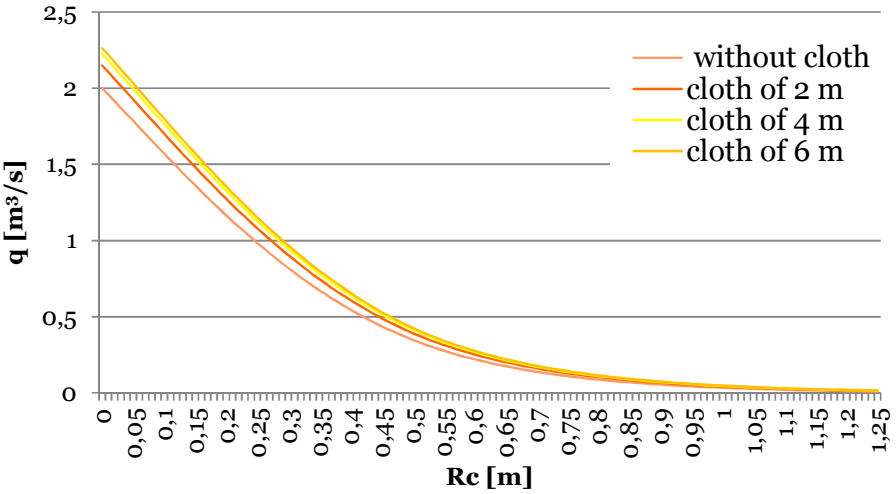


**Figure 5. Overtopping for different ramp´s lengths; Hs=0.6m, T=3s, device length =13.5 m.**

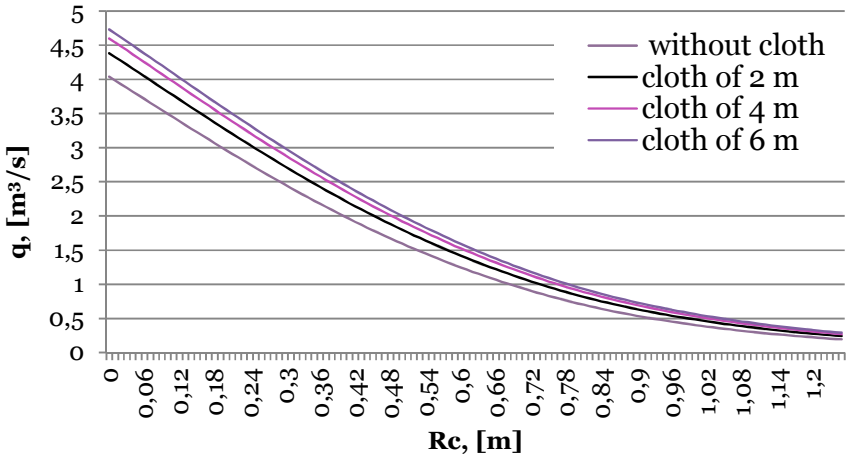


**Figure 6. Overtopping for different ramp´s lengths; Hs=1.0 m, T=3.6 s, device length =13.5 m.**

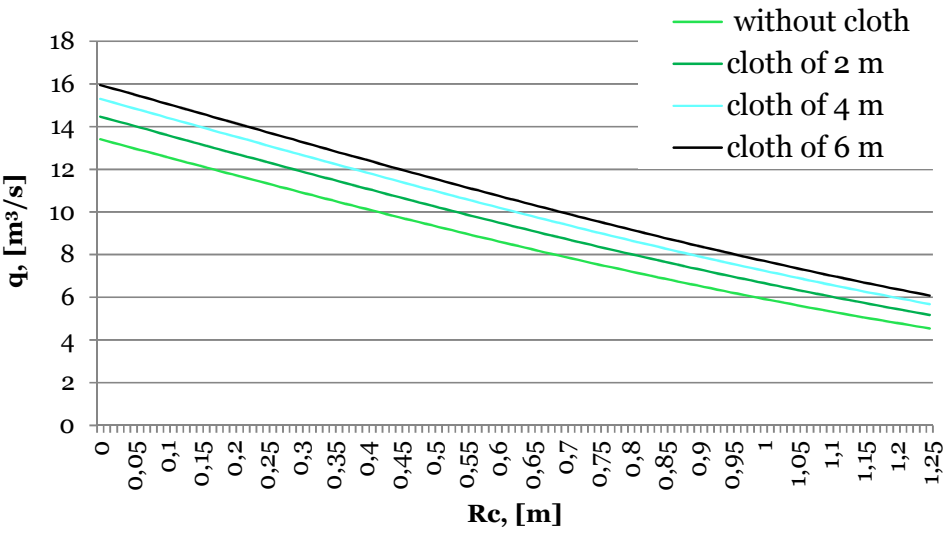


**Figure 7. Overtopping for different ramp´s lengths; Hs=2.4 m, T=5.1 s, device length =13.5 m.**

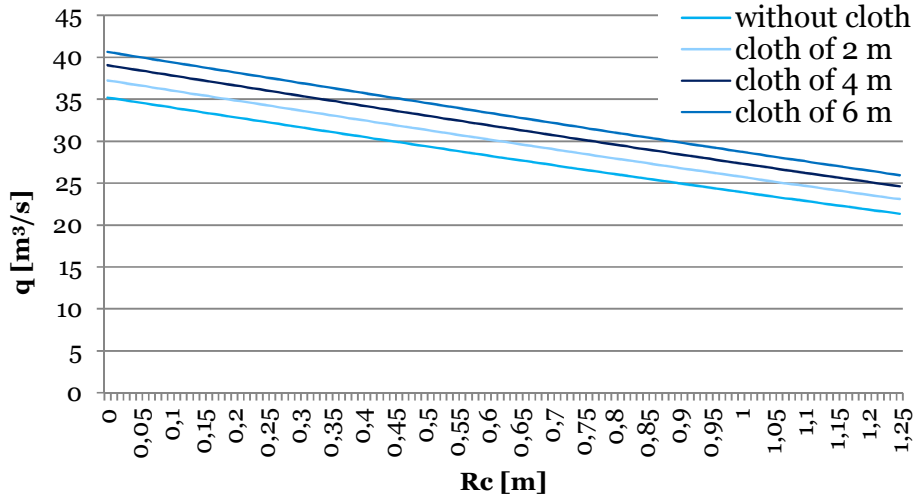


**Figure 8. Overtopping for different ramp´s lengths; Hs=4.8 m, T=6.9 s, device length =13.5 m.**

**Table 1. Overtopping flow rates [m3/s/m] in different wave conditions for Rc =1.25 m and varying cloth length.**

| dr [m] | 0,0 | 2 m length=0,8 draft | 4 m length=1,5 m draft | 6 m length=2,3 m draft |
|---|---|---|---|---|
| Hs=0.6 m, Rc=1.25 m | **0,0008** | **0,0010** | **0,0011** | **0,0012** |
| Hs=1.0 m, Rc=1.25 m | **0,0142** | **0,0178** | **0,0200** | **0,0214** |
| Hs=2.4 m, Rc=1.25 m | **0,3360** | **0,3834** | **0,4208** | **0,4503** |
| Hs=4.8 m, Rc=1.25 m | **1,5817** | **1,7103** | **1,8232** | **1,9223** |

## *2.3 Influence of the slope angle*

Finally the influence of the slope angle is presented. In total four different slope angles have been considered: 23° as suggested by the developer, 15°, 30 ° and 35°.

The higher overtopping occurs for angles between 23° and 35°. While graphically there is a noticeable difference for the case featuring 15° and generating the lowest overtopping, almost no difference shows for the remaining cases across all the wave conditions (Fig.9-12). This suggests there is almost no difference on the overtopping if any angle between 15˚ and 35˚ is chosen. As for the previous parameters, the overtopping is larger for higher waves following a linear trend. For lower waves the overtopping is zero or negligible until the crest Rc is lower enough to allow the water in the incoming waves to overtop it and be stored in the reservoir. In average, passing from a slope angle of 15˚ to something between 23˚ and 35˚ gives an increase on overtopping volumes of 8%, while changing from 23˚ to 30˚ or 35˚ only gives maximum 3% more.

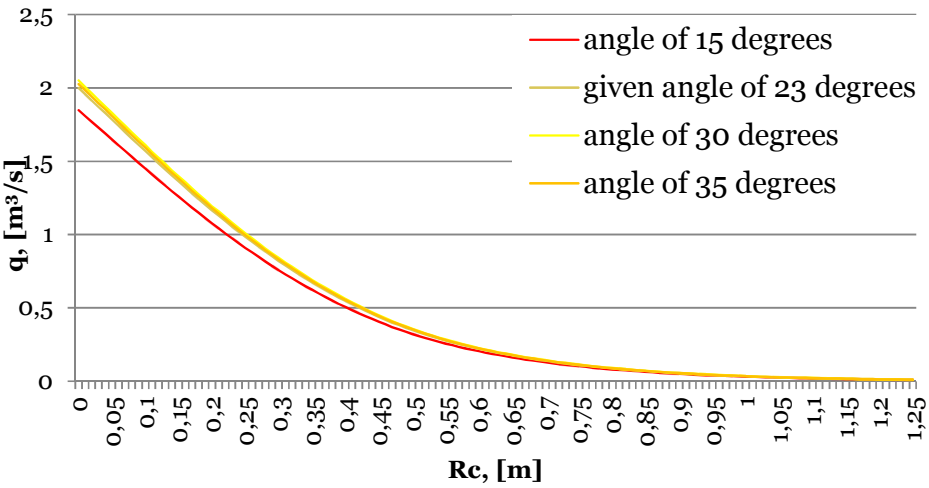


**Figure 9. Influence of slope angle on the overtopping flow rates in different wave conditions, Hs=0.6 m, Tp=3 s, device length 13.5 m.**

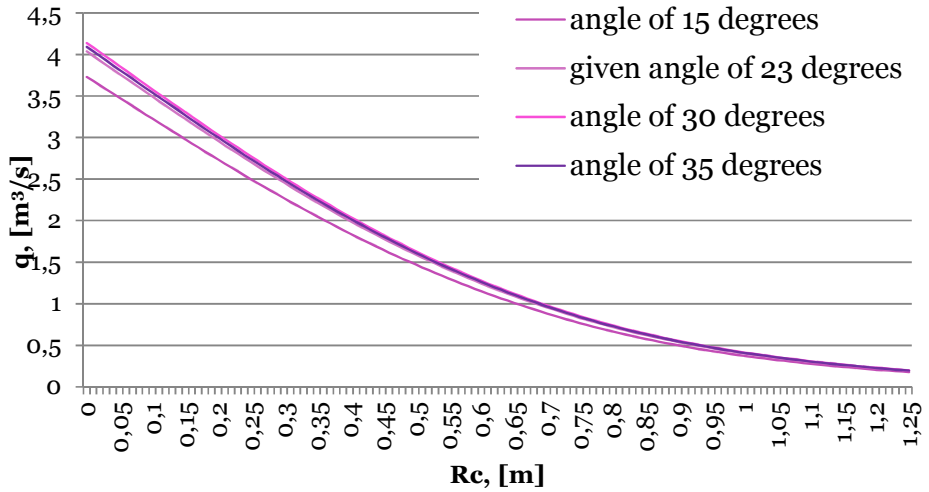


**Figure 10. Influence of slope angle on the overtopping flow rates in different wave conditions, Hs=1.0 m, Tp=3.6 s, total device length 13.5 m.**

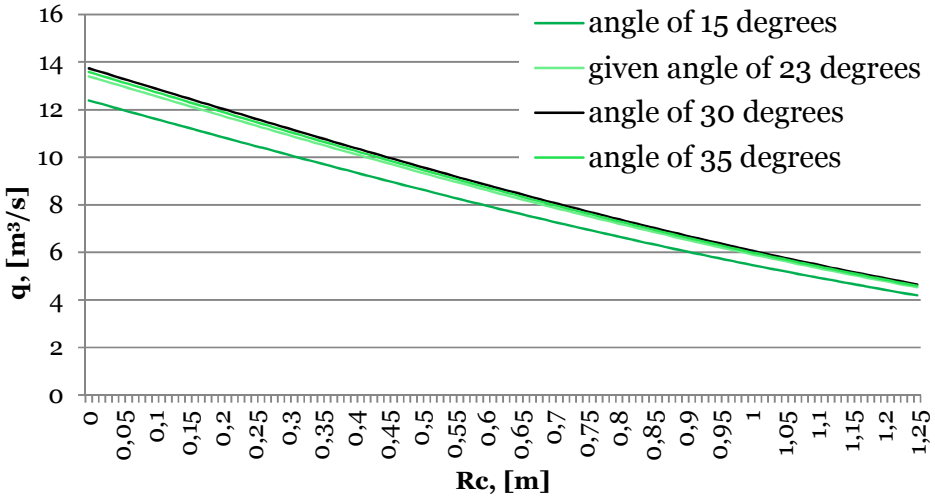


**Figure 11. Influence of slope angle on the overtopping flow rates in different wave conditions, Hs=2.4 m, Tp=5.1 s, total device length 13.5 m.**

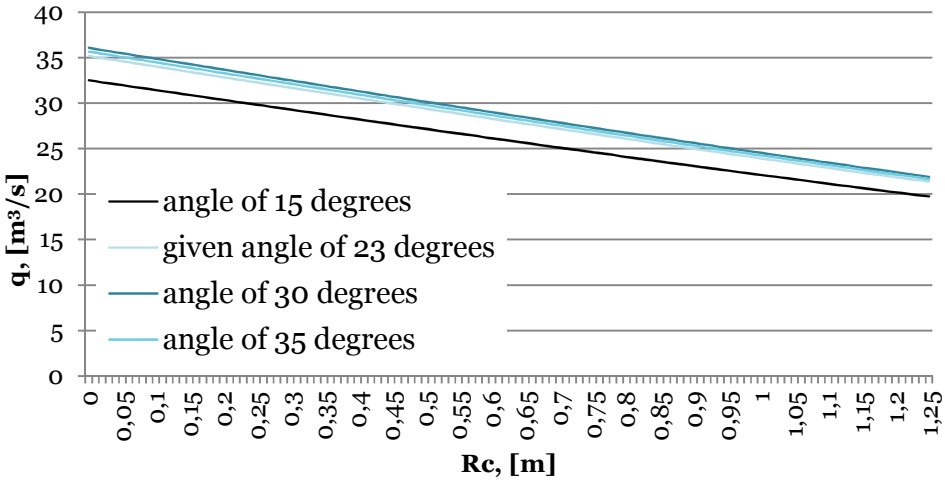


**Figure 12. Influence of slope angle on the overtopping flow rates in different wave conditions, Hs=4.8 m, Tp= 6.9 s, total device length 13.5 m.**

## *2.4 Conclusions*

1_Basic geometry, with slope angle of 23˚, without ramp extension.

For Hs=0.6 m, Tp=3.0 s, the overtopping q is negligible for Rc>0.45 m.
For Hs=1.0 m, Tp=3.6 s, the overtopping q= is negligible for Rc>1.15 m.
For Hs=4.8 m, Tp=6.9 s, Rc=1.25 m, dr=0, then q=1.55 m³/s/m.
For Hs=4.8 m, Tp=6.9 s, Rc=0.55 m, dr=0.70, then q=2.1 m³/s/m.

2_Influence of extending the ramp.

Extending the ramp increases the overtopping and the effect is more beneficial for lower seas states or higher crest levels.

In average, for Hs=0.6 m, ramp extension of 2 m increases the overtopping of 16.5% across different crest levels, compared to the case without ramp extension. For Hs=4.8 m, ramp extension of 2 m increases the overtopping of 6.9 % across different crest levels.

In average, for Hs=0.6 m, ramp extension of 6 m increases the overtopping of 29% across different crest levels, compared to the case without ramp extension. For Hs=4.8 m, ramp extension of 6 m increases the overtopping of 13 % across different crest levels.

For Rc=1.25, Hs=2.4 m, 6 m ramp extension generates a 34% bigger overtopping than in the case without ramp extension. For Hs=4.8 m, ramp extension of 6 m generates a 21% bigger overtopping compared to the case without ramp extension.

3_Influence of slope angle.

Passing from 23˚ to 30˚ will generate an increase in overtopping of around 3%.

Not consistent different on the overtopping volumes is then expected for slope angles within 23˚ and 35˚. This range of angles is the optimal for maximization of overtopping. Bigger slope angles would prevent water for overtopping the crest while smaller slope angel would induce breaking and loss of overtopping volumes.

# 3 Estimation of pipe capacity as function of water level in the reservoir

The pipe will be several meters long, going roughly from the surface to the bottom of the sea where there is lack of oxygen. It is foreseen that the pipe length will be between 50 and 80 meters, depending on the location.

Such a long pipe like the one that will be used for the WEBAP will have losses due to its length and roughness, as well as inlet and outlet losses. The issue of difference in water density must also be taken into account. The Baltic Sea receives abundant freshwater runoff from the surrounding land and is therefore less salted than the ocean water. Another factor influencing the water density in its temperature. Measurement of temperature and salinity at different depth (from 0 to -80 m) in the years 2006 and 2007 have been used to calculate differences in water density and necessary head to overcome density differences. The following expression to calculate the water density has been used (McCutcheon, et all. 1993):

$$\rho = \rho + AS + BS^{3/2} + CS^2 \quad (4)$$

where:
A = 8.24493E-1 - 4.0899E-3*T + 7.6438E-5*T^2 -8.2467E-7*T^3 + 5.3675E-9*T^4
B = -5.724E-3 + 1.0227E-4*T - 1.6546E-6*T^2
C = 4.8314E-4
T = temperature (degrees in Celsius)
S = salinity (gr/Kg)

It is possible to individuate a consistent gradient after 40 m water depth (table 2).

**Table 2. Average changes in water density depending on depth for the years 2006 and 2007.**

| water depth [m] | 0 | 5 | 10 | 15 | 20 | 30 | 40 | 50 | 60 | 70 | 80 |
|---|---|---|---|---|---|---|---|---|---|---|---|
| average water density [kg/m$^3$] | **1005,3** | **1005,3** | **1005,3** | **1005,4** | **1005,7** | **1006,0** | **1006,5** | **1007,7** | **1010,1** | **1011,8** | **1012,2** |

The necessary head to overcome density differences has been calculated with the expression:

$$\Delta h = \frac{\sum_{i=1}^{n} \rho_i L_i - \rho_1 D}{\rho_1} \quad (5)$$

Where ρi is the density of the "i" layer, Li is the length of the "i" layer (5 m until 20 m water depth and 10 m for the deeper layers), ρ1 is the density of the surface water and D is the pipe diameter =2.05 m. For a pipe with this characteristics and total length of 50m, the necessary head is 0.04 m, while a for 70 m and 80 m pipe, the necessary heads are 0.13 m and 0.19 m respectively.

Head loss hf due to friction in a pipe can be calculated using the Darcy-Weisbach equation:

$$h_f = \left( K_e + \frac{fL}{D} + K_{exit} \right) \frac{V^2}{2g} \quad (6)$$

where:
$h_f$ - head loss

$f$ - friction factor
$L$ - length of pipe
$D$ - diameter of pipe
$K_e$ - entrance loss coefficient
$K_{exit}$ - exit loss coefficient
$V$ - velocity of fluid
$g$ - acceleration due to gravity

For turbulent flow, $f$ is determined from Colebrook-White equation:

$$\frac{1}{f} = -2\log\left(\frac{k}{3.7D} + \frac{2.5}{\frac{VD}{\upsilon}\sqrt{f}}\right) \tag{7}$$

where:
$k$ - internal roughness of the pipe
$\upsilon$ - kinematic viscosity of the fluid

From equations 5 and 6 the flow velocity v has been calculated. The pipe capacity is then the function of v and area of the pipe section A:

$$Q = A \cdot v \tag{8}$$

For a 70 m long pipe of 2.05 m diameter, the pipe capacity has been calculated for different reservoir heads and 2 roughness associated with different materials (Fig. 13). The hf is equal to the total head in the reservoir minus the necessary head to overcome density differences at 70 m water depth (=0.13 m).

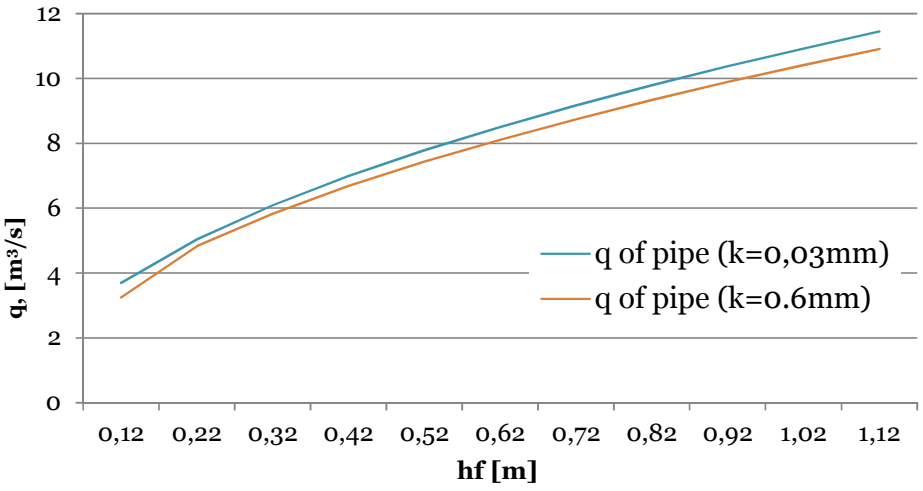


**Figure 13. Pipe capacity for different heads hf and materials for a pipe 70 m long and 2.05 m diameter, 13. 5 m long device.**

## *3.1 Conclusions*

Differences in water column density and losses due to the length of the pipe must be won by the driving head in order to have the pump mechanism working. The minimum head necessary is 0.13 m for a 70 m long pipe, 0.19 m for an 80 m long pipe while only 0.04 m are needed for a 50 m long pipe. These are also the water depths that will not drain out of the reservoir.

# 4 Laboratory testing and model

The laboratory tests investigated mooring forces, movements of the floating body and the functioning of the "pump mechanism" to take the overtopping water down to the sea bottom through the pipe. Tests have been carried out in the deep wave tank of the Hydraulic and Coastal Engineering Laboratory of Aalborg University. The tests are in scale 1:25. The model of the WEBAP device has been constructed at Aalborg University under indication of the constructors. Particular attention has been given to the dimensioning of the pipe (see Chapter 3).

## *4.1 Laboratory set up*

Full scale dimensions have been given by the developer. The model in scale 1:25 (Froude scale) has been realized in light metal and foam. The extension of the ramp is realized with rubber cloth stretched on two lateral metal support fixed to the ramp. The tube is fixed to the main body by mean of a rigid tube that is also hosting the propeller for rotational speed measurement (Fig. 14).

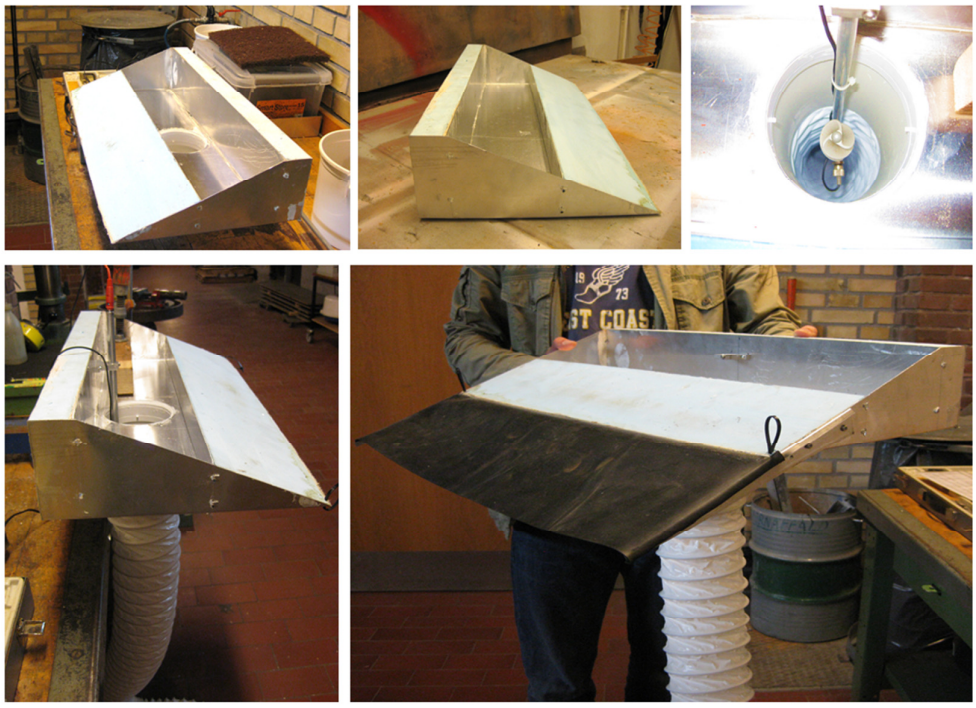

**Figure 14.Construction progress of WEBAP model in scale 1:25 at Aalborg University.**

The pipe was realized with a flexible plastic tube kept vertical by weights attached to the bottom side. Directly scaling the pipe dimensions with Froude law would be imprecise as the flow process is not dominated by gravity forces (as in wave's processes) but by viscous forces that would require a different scaling law (not Froude but Reynolds). Moreover, it is difficult to scale down properly the roughness of the material when going to the laboratory. It is said that scaling down directly the dimensions of the pipe (L=70 m and D =2.05 m) with Froude law would give pipe dimensions that would allow a smaller flow; this as result of scaling limitations. Keeping this in mind, the final pipe used in the model is 1.7 m long, has a diameter of 0.10 m and a roughness k=0.003. The capacity of the pipe is plotted in Fig. 15, together with other pipes taken into consideration for the laboratory model. The final model dimensions are presented in Fig. 16.

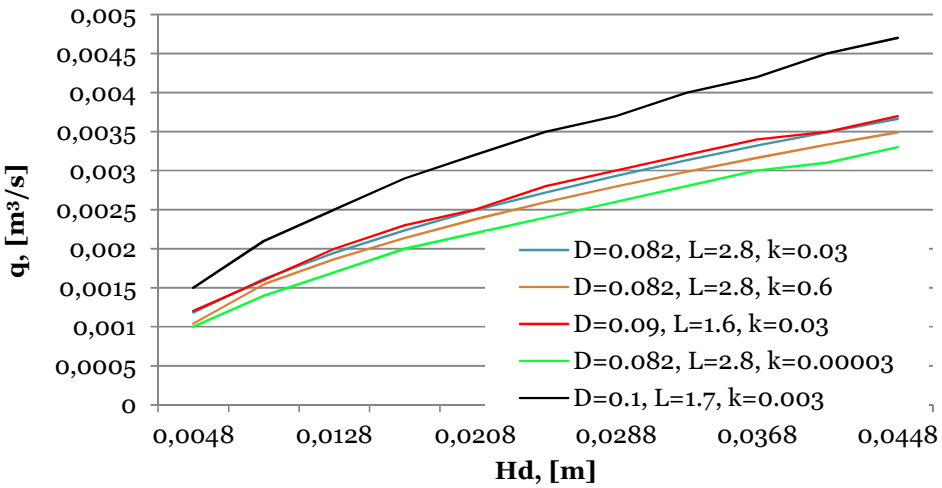


**Figure 15. Different pipe capacities for the laboratory model.**

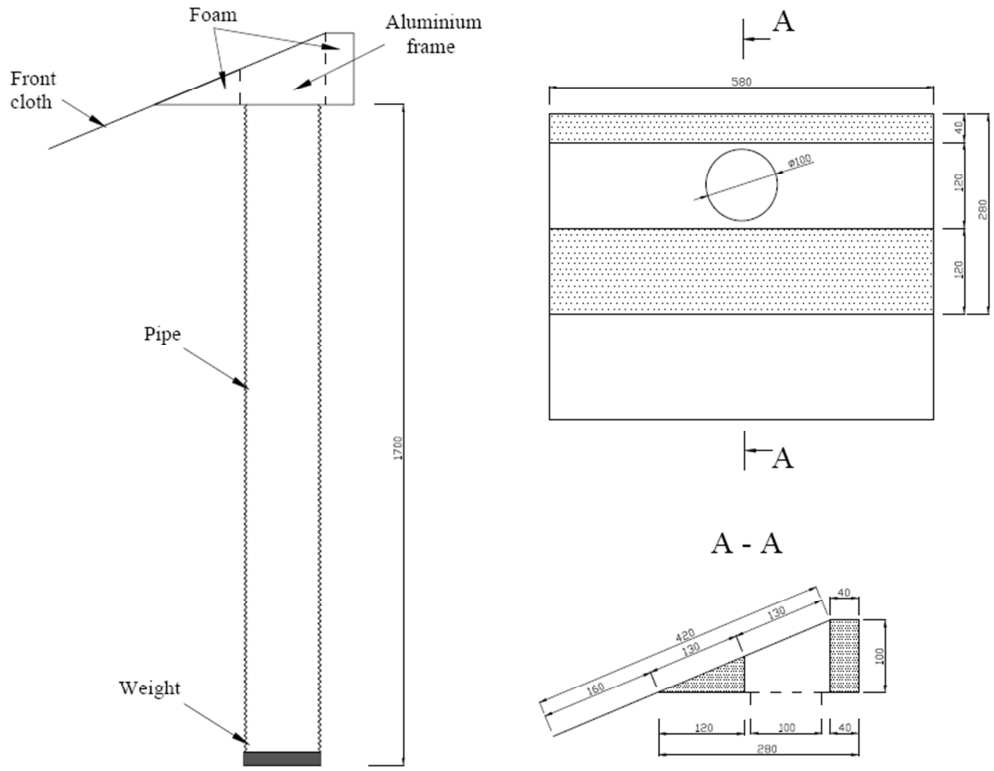


**Figure 16. Measures of the model, scale 1:25, measure in mm.**

The model (Fig. 17) was placed in the middle of the deep 3D wave tank, in the deep section with water depth d=2.15 m and equipped with front and rear mooring to avoid undesired movement during and after testing.

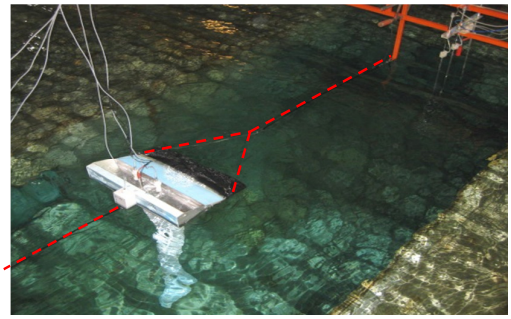

**Figure 17. Moorings set up.**

## *4.2 Measuring equipment*

Three wave gauges (sample frequency: 25 Hz) have been installed in front of the system to measure incident and reflected waves, generated by software AwaSys 5. The model has been equipped with (Fig. 18):

- No. 2 load cells on the mooring lines, sample frequency: 25 Hz.
- No. 1 MTi to measure the movement of the body under waves excitation i.e. roll, pitch and yaw, as well as accelerations in the three directions, sample frequency 25 Hz (A appendix).
- No. 1 propeller to measure rotational speed proportional to flow velocity inside the pipe.
- No. 2 small wave gauges in the reservoir to measure the water level.

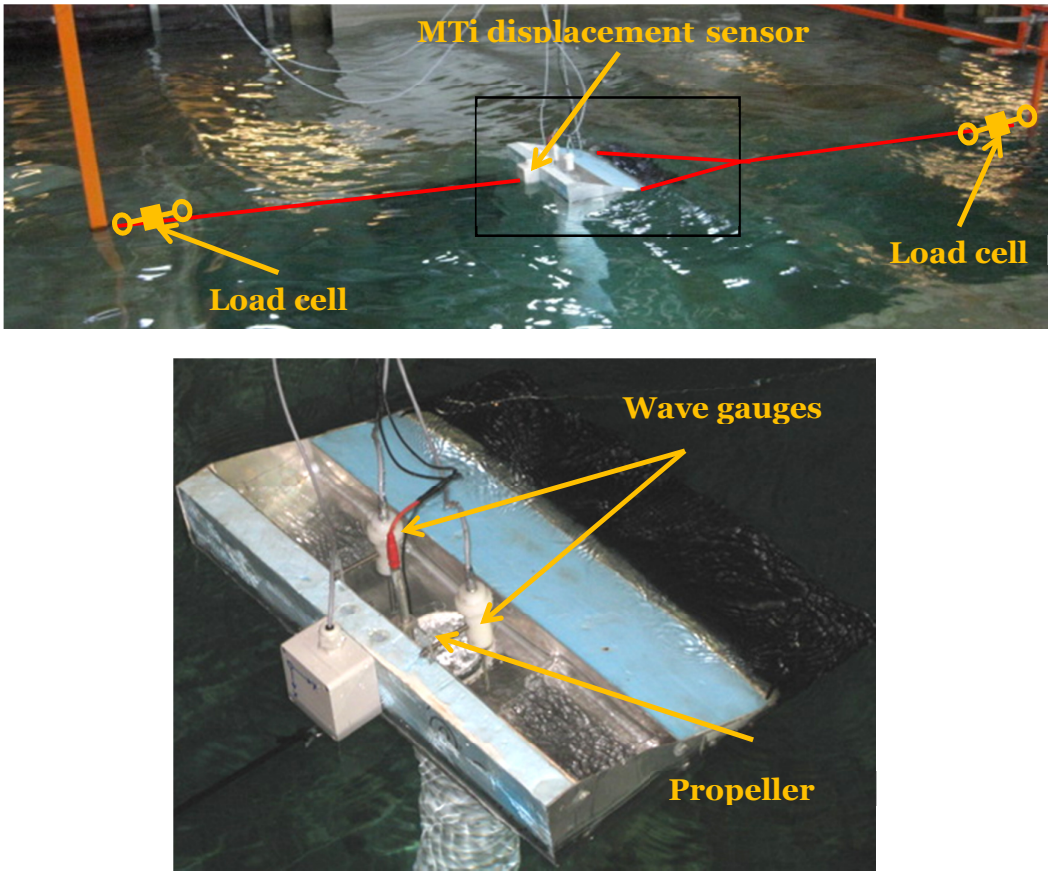


**Figure 18. Model setup.**

## *4.3 Wave characteristics*

The device was tested under 2D irregular waves (Jonswap spectrum 3.3) for the conditions in table 3 supplied by the developer. Length of each test is 30 minutes. The water depth was 1.95 m for half of the tests and 2.15 m for the other half. This is just mentioned for the sake of reporting but the parameter water depth was investigated in the present report.

**Table 3. Input waves used in the laboratory and corresponding full scale.**

| | PM spectrum (PM), 1:25 | | PM spectrum (RW); 1:1 | |
|---|---|---|---|---|
| | Hs [m] | Tz [s] | Hs [m] | Tz [s] |
| W1 | 0,024 | 0,6 | 0,6 | 3 |
| W2 | 0,04 | 0,72 | 1,0 | 3,6 |
| W3 | 0,096 | 1,02 | 2,4 | 5,1 |
| W4 | 0,192 | 1,38 | 4,8 | 6,9 |

Useful relations between wave parameters are:

$$H_{m0} = 4 \cdot \sqrt{m_0} \quad (9)$$

Where:

mn= $\int_0^{+\infty} f^n \cdot E(f) df$ = n'th order spectral moment, f = frequency [$s^{-1}$], E(f) = Spectrum energy density depending on the frequency [$m^2 s$].

Hm0 is normally used instead of Hs when breaking waves occur and the Rayleigh distribution function that normally describes the wave heights may not be reliable.

$$Tp = 1.4\ Tz \quad (10)$$

The peak period Tp is normally used as input for wave spectrum generation. As the significant wave height is the average of the wave heights of the one third highest waves, the significant wave period is the average of the wave periods associated with one-third highest waves.

## *4.4 Conclusions*

The WEBAP model is scale 1:25 has been constructed following the developer´s design.

The model has been instrumented in order to measure mooring forces, movements and rotational speed of the propeller under the action of the flow drained down out of the reservoir through the pipe. In addition two wave gauges in the reservoir where used to monitor and detect possible spill out water from the reservoir that would indicate an insufficient pump capacity.

The model has been installed in the deep water wave tank secured by two mooring lines.

Some difficulties have been encountered on respecting the buoyancy requirements due to the small size of the model and the height number of instruments on the floating body. Nevertheless by adding extra foam and using MTi measuring device which is small and light, a minimum draft of 0.022 m, corresponding to 0.55 m full scale has been achieved.

# 5 Results and analysis

The data acquisition has been handled by WaveLab3 (Fig 19). The same software allowed also the analysis of the mooring forces, generated wave and water levels inside the reservoir. Seven acquisition channels where used:

- 1 and 2 = rear and front load cells
- 3, 4 and 5 = wave gauges in the basin
- 6 and 7 = wave gauges inside the reservoir

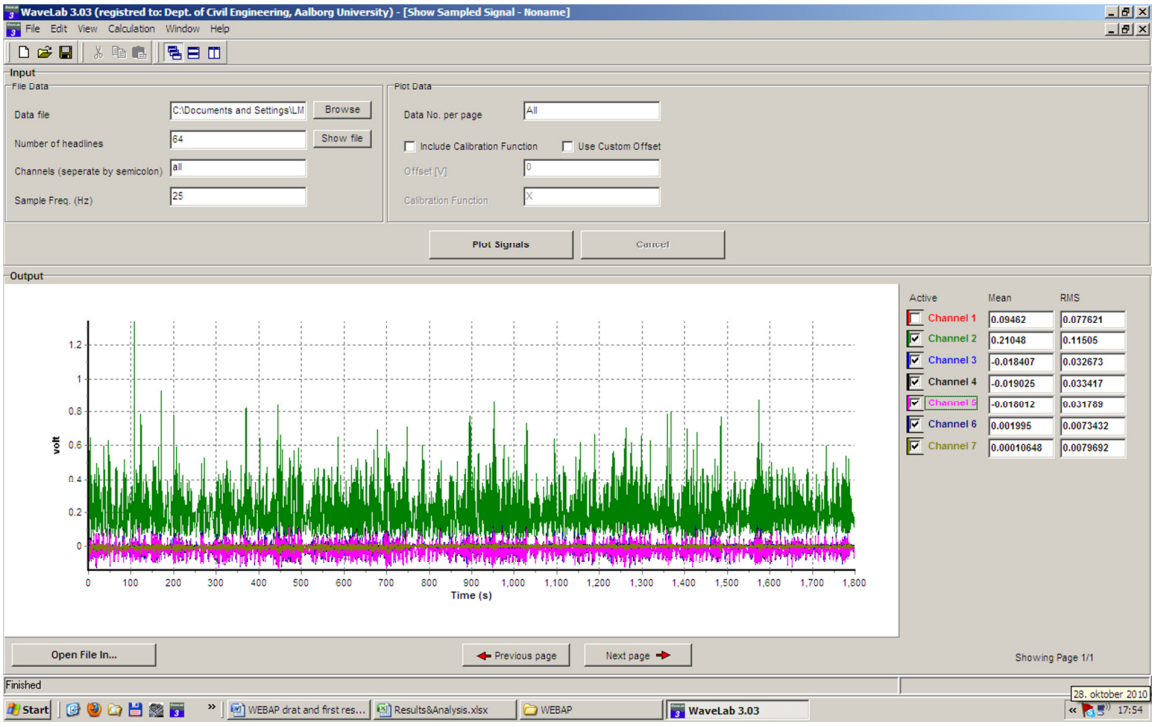


**Figure 19. Snapshot from WaveLab, plot data.**

The propeller revolutions were noted down at regular intervals of time during the tests.

The movement data where handled by the MTi software in a different computer. Outputs were: pitch, roll, yaw and accelerations in the three reference directions. The movements´ analysis has been carried out with a Matlab routine. Indeed, the Mti instrument acquires pitch, roll, yaw and the accelerations in the three dimensions. The last ones needed to be double integrated to obtain the displacements.

## *5.1 Generated waves and tested configurations*

A total of 18 tests have been carried out with different model configuration and wave conditions. The length of each test was 30 minutes.

Two different stiffnesses have been used indicated with S1 and S2, being S2 the stiffer one.

Few tests have also been carried out with an increased draft, obtained by applying little extra weight on the structure and sinking it. The standard tested draft was as small as possible dr1 = 0.55

m corresponding to a crest Rc1 = 0.70 m. while increased draft dr2=0.93 m corresponding to a crest of Rc2=0.32 m (tests´ tag _B2_).

Finally a fix configuration was also tested in order to identify the effect of motion on the overtopping (tests´ tag _Fix_).

The ramp length utilized during the tests corresponds to 4 m in full scale.

Maximum generated Hm0 is 4.220 m, with Tp=8.715 s, corresponding roughly to wave condition W4. All the tests and respective measured/generated wave are presented in Table 4.

**Table 4. Generated waves, translated in full scale.**

| File name | Reflection coefficient = Hm0 reflected/Hm0 incident | Hm0 [m] | Tp [s] |
|---|---|---|---|
| **Water depth 48.25 m ↓** | | | |
| *_W1_S1_Free_01.dat | 0.1805 | 0.245 | 3.828 |
| *_W2_S1_Free_01.dat | 0.1347 | 0.578 | 4.655 |
| *_W3_S1_Free_01.dat | 0.1035 | 1.900 | 6.400 |
| *_W41_S1_Free_Hs0.12Tp1.5_01.dat | 0.1113 | 2.407 | 7.185 |
| *_W42_S1_Free_Hs0.192Tp1.5_01.dat | 0.1161 | 3.430 | 7.875 |
| *_W44_S1_Free_Hs0.21Tp1.5_01.dat | 0.1145 | 3.600 | 7.875 |
| **Water depth 53.75 m ↓** | | | |
| *_W3_S1_D0605_Free_01.dat | 0.09756 | 2.033 | 6.300 |
| *_W4_S1_D0605_Free_01.dat | 0.09284 | 4.190 | 8.715 |
| *_W3_S2_Free_D0605_01.dat | 0.09863 | 2.021 | 6.300 |
| *_W4_S2_Free_D0605_01.dat | 0.09476 | 4.220 | 8.715 |
| *_W2_S2_B2_Free_D0605_01.dat | 0.1569 | 0.658 | 4.602 |
| *_W3_S2_B2_Free_D0605_01.dat | 0.1006 | 2.006 | 6.300 |
| **Fix ↓** | | | |
| *_W2_B2_Fixed_D0605_01.dat | 0.2218 | 0.649 | 4.405 |
| *_W3_B2_Fixed_D0605_01.dat | 0.125 | 2.057 | 6.300 |

Nine tests have been realized with S1, dr1 and water depth of 48.25 m; one of these failed because the pipe detached during W4 and an other because the water depth at the paddles was not sufficient to generate W4. Two tests have been run with S1, dr1 and water depth of 53.75 m. Four tests have been run with S2, dr1 and water depth equal to 53.75 m; one test failed because the pipe detached from the main body, again with W4. Three tests have been run with a fixed structure, dr2 and water depth of 53.75 m. In the overall, two tests presented problems in the acquired signal therefore have been rejected.

Figure 20 reports the variance spectrum of test W4_S2_Free_D0605_01 from the frequency domain analysis while in Figure 21 is reported the wave height distribution from the time domain.

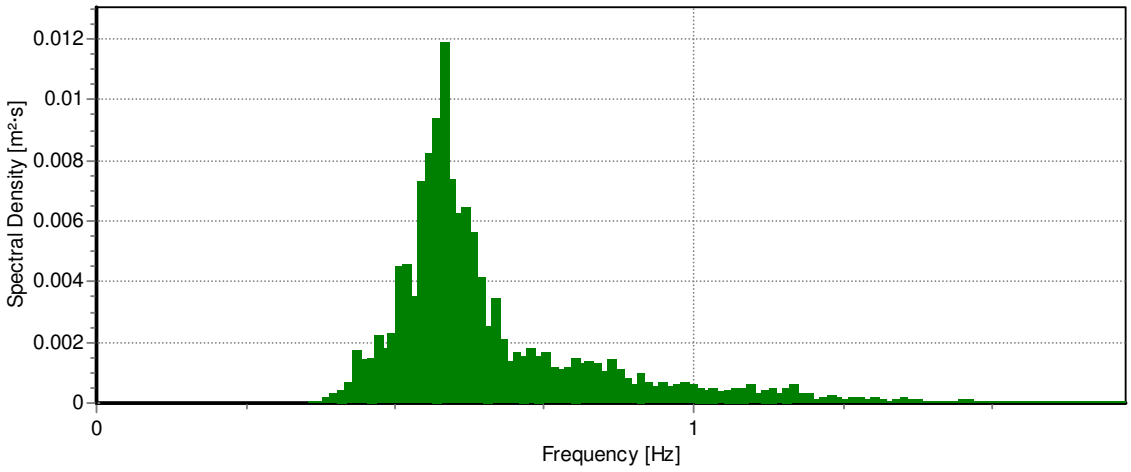


**Figure 20. Variance Spectrum, test W4_S2_Free_D0605_01.**

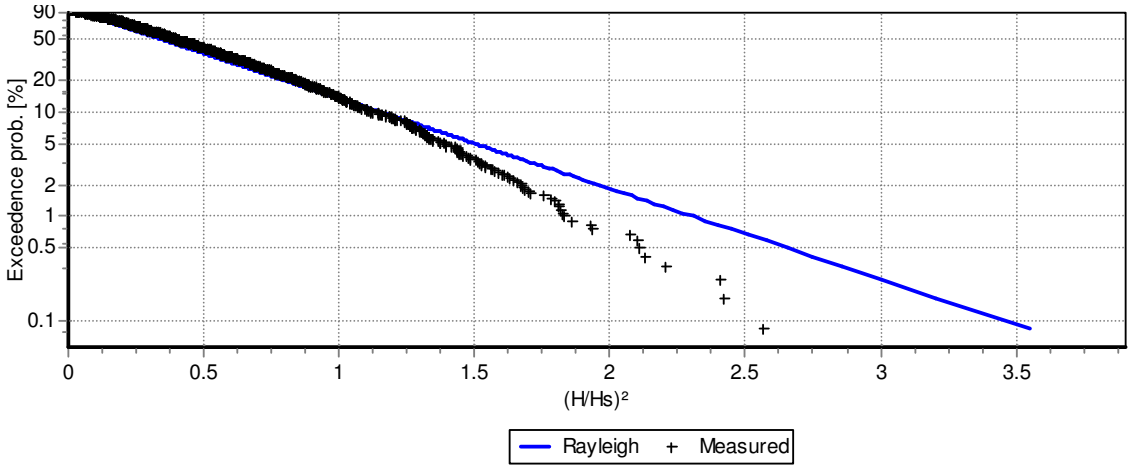


**Figure 21. Wave height distribution, test W4_S2_Free_D0605_01**

## *5.2 Moorings characteristics*

Mooring forces are presented in terms of statistical peak force parameters conforming to the Rayleigh distribution F1/250 obtained from Wavelab time series analysis of the signal measured by load cells on the mooring lines. It is very important to notice that design wave height is defined as the highest wave in the design sea state at the location just in front of the structure. If seaward of a surf zone Goda (1985) recommends for practical design a value of 1.8 Hs to be used corresponding to the 0.15% exceedence value for Rayleigh distributed wave heights. This corresponds to H1/250, mean of the heights of the waves included in 1/250 of the total number of waves, counted in descending order of height from the highest wave.

The mooring system (front and back) has been realized with two elastic rubber ropes fixed to the model at one side and to a steady point of the basin in the other. The unloaded ropes´ length was 1.78 m and 1.21 m for the front and rear line respectively in configuration S1 (corresponding to 44.5 and 30.25 m in real scale). The stiffer configuration was realized by shortening the ropes. In configuration S2 the lengths were 1.36 m and 0.79 m for front and rear line respectively

(corresponding to 34m and 19.5 m in full scale). The characteristic of the two tested stiffness's are in Fig. 22 and 23 for front and rear mooring respectively. The stiffness is then the inclination of the curves.

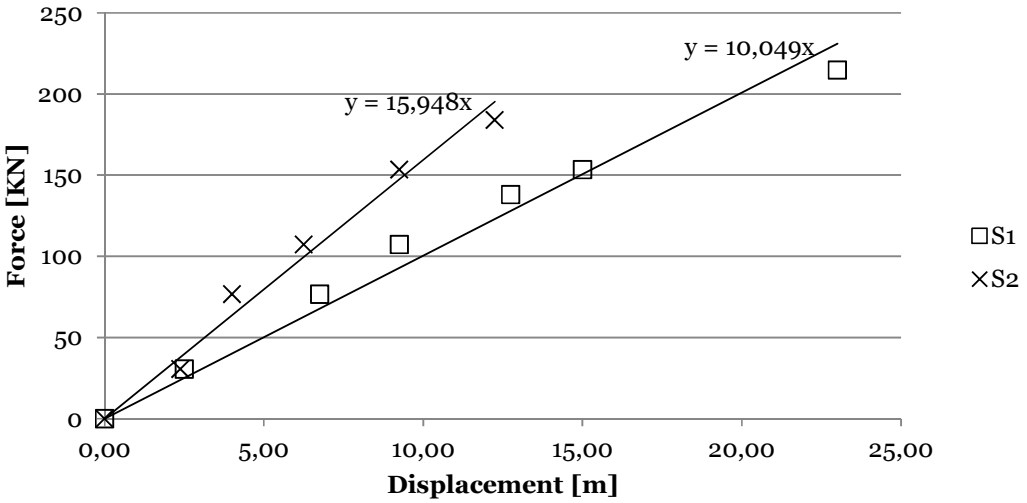


**Figure 22. Tested stiffnesses, full scale, front line.**

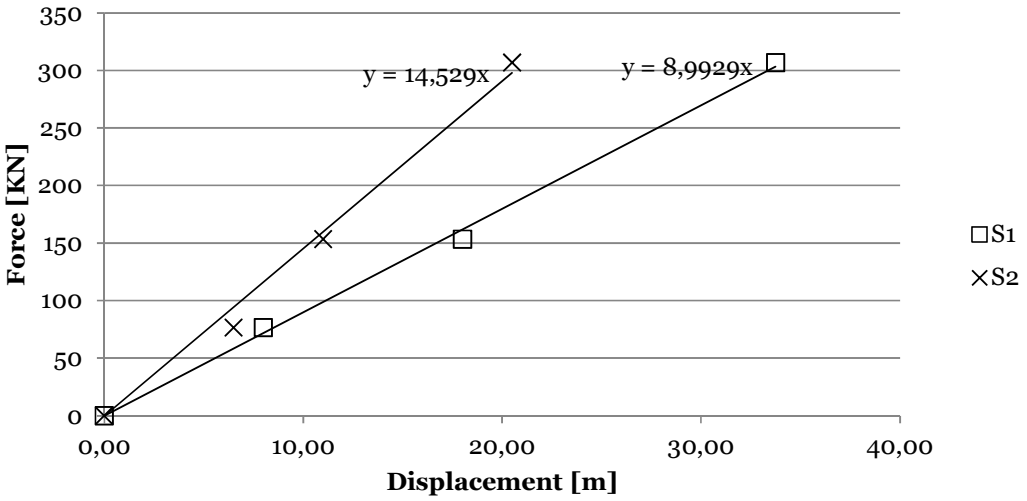


**Figure 23. Tested stifnesses, full scale, rear line**

When the mooring lines have been fixed, the system acquired a pretension. This was 17.5 KN for S1 and 144.0 KN for S2, full scale. The combined action of the two mooring lines has then been presented in Fig. 24 and 25. When the acting force is within the limits of the pretension, slack will not occur. For mooring system S1 this allows movements up to 3.5 m backwards and 3.9 m forwards (surge) without slacking. For the mooring system S2, 18.1 m and 19.8 m movements are allowed backward and forwards respectively.

The force-displacement system is then regulated by the characteristic of the singular rear and mooring lines only when the pretension is overcome. Otherwise, the mooring system follows a combined action of front and rear lines represented by the central green line in Fig. 24 and 25.

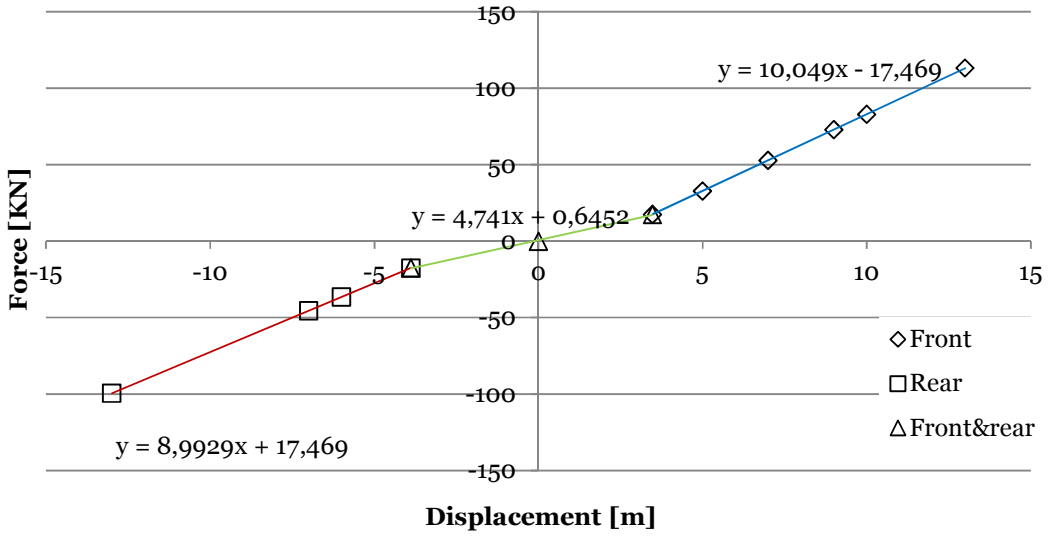


**Figure 24. Combined action of front and rear mooring, S1, full scale.**

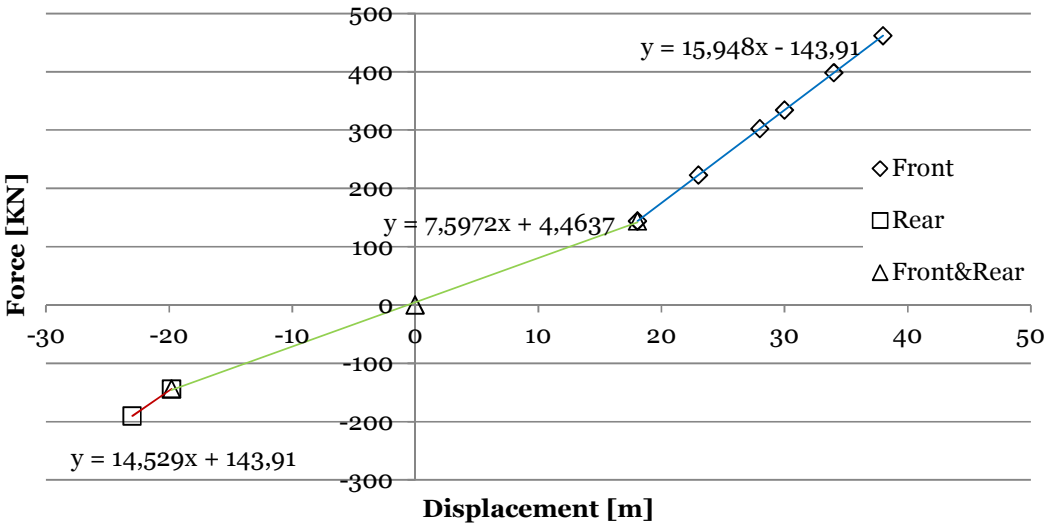


**Figure 25. Combined action of front and rear mooring, S2, full scale.**

## *5.3 Free oscillation tests*

The free oscillation tests are performed in order to find the natural frequency of the floating body which characterized its shape and hydrodynamic behavior. For the free oscillation tests, the stiffness S1 was used.

The device is “dragged” by pulling the rear mooring (in case of surge) and let free to move while recording the movements. In the case of heave, the device is sunk and then let free to move, while for the pitch the device has been tilted by pulling down the front part of the structure.

The results show a natural frequency of 2.5 seconds for surge, 20 seconds for heave and 2.8 seconds for the pitch (Fig. 26-28).

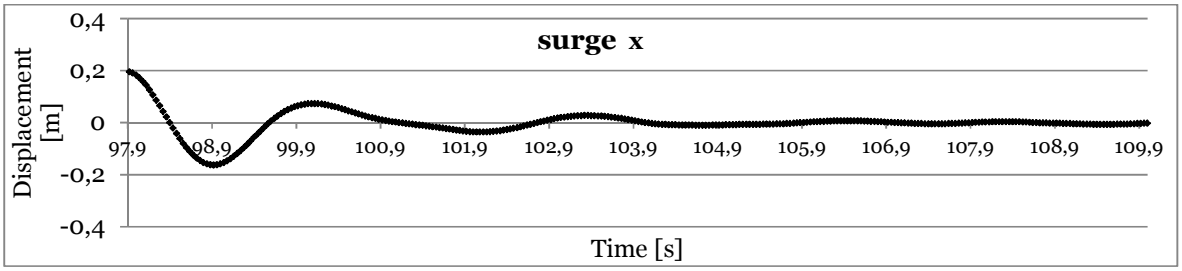


**Figure 26. Free oscillation tests results for surge, model scale.**

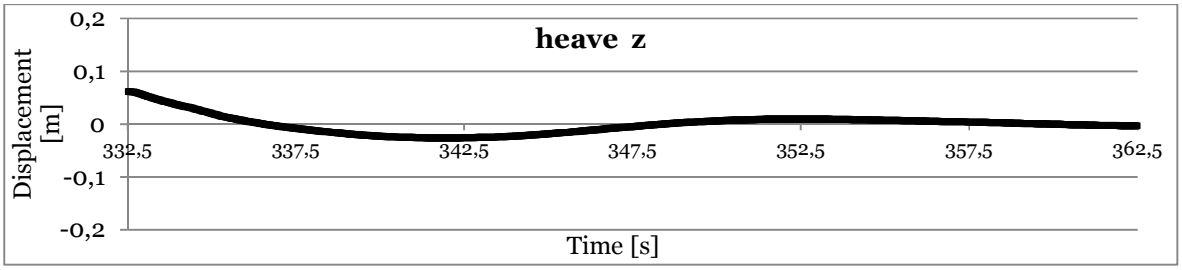


**Figure 27. Free oscillation tests results for heave, model scale.**

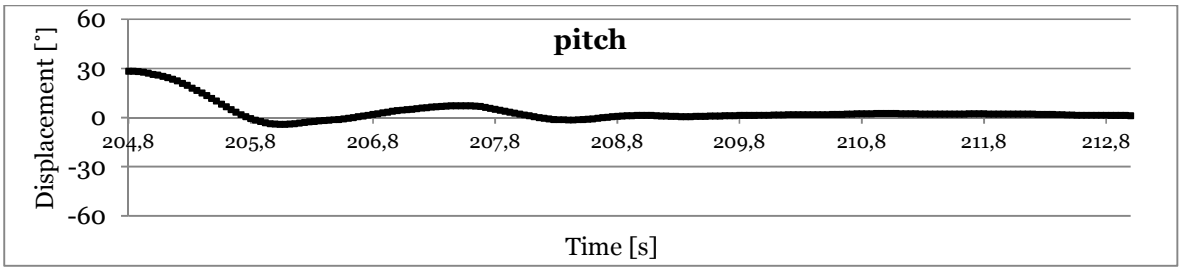


**Figure 28. Free oscillation tests results for pitch, model scale.**

For the surge it has been noticed that when the structure was let free after it was pulled from the rear mooring, while the device was smoothly moving backward, it was getting stuck moving forward due to the extension of the front ramp. This can be noticed in seconds 99.9-101.9 in Fig. 17 where the device is moving forward. The device is moving forward also between seconds 97,9 and 98.9 but the dragging force of the mooring recalling the device forward is stronger than the friction generated by the ramp as the device has just been released after the rear mooring has been pulled.

For the heave, a quite long natural frequency was found. This could be justified by the presence of the pipe.

The pitch is almost independent of the mooring system. We can notice that device tilts easier forward than backwards, generating bigger displacements on the positive side of the Y axis. Indeed,

the oscillations on the positive side of the Y axis represent the tilting of the front, while the tilting of the back results blocked by the presence of the pipe which is in the rear side of the structure.

## *5.4 Mooring forces*

Forces are here presented in full scale through the key statistical parameter F1/250 and without the pretension. All the results on mooring forces are reported in full scale in Table 5.

**Table 5. Overall results on mooring forces.**

| | File name | Wave conditions | | Mooring [KN] | |
|---|---|---|---|---|---|
| | | Hm0 [m] | Tp [s] | rear | front |
| d=water depth= 1.95 m | *_W1_S1_Free_01.dat | 0.25 | 3.83 | 2.90 | 4.90 |
| | *_W2_S1_Free_01.dat | 0.58 | 4.65 | 7.44 | 17.84 |
| | *_W3_S1_Free_01.dat | 1.90 | 6.40 | 13.37 | 29.98 |
| | *_W41_S1_Free_Hs0.12Tp1.5_01.dat | 2.41 | 7.19 | 29.20 | 42.49 |
| | *_W42_S1_Free_Hs0.192Tp1.5_01.dat | 3.43 | 7.88 | 43.33 | 64.95 |
| | *_W44_S1_Free_Hs0.21Tp1.5_01.dat | 3.60 | 7.88 | 47.49 | 78.17 |
| | | | | | |
| d=water depth= 2.15 m | *_W3_S1_D0605_Free_01.dat | 2.03 | 6.30 | 16.69 | 31.88 |
| | *_W4_S1_D0605_Free_01.dat | 4.19 | 8.72 | 46.66 | 89.45 |
| | | | | | |
| | *_W3_S2_Free_D0605_01.dat | 2.02 | 6.30 | 20.70 | 42.64 |
| | *_W4_S2_Free_D0605_01.dat | 4.22 | 8.72 | 51.11 | 102.86 |
| | *_W2_S2_B2_Free_D0605_01.dat | 0.66 | 4.60 | 6.88 | 14.63 |
| | *_W3_S2_B2_Free_D0605_01.dat | 2.01 | 6.30 | 21.83 | 42.00 |

The maximum F1/250 obtained is on the front mooring for the S2 and draft of 0.55 m below sea water level, under Hm0=4.22 m. This force corresponds to F1/250=102.9 KN. The second highest force is F1/250=89.5 KN and occurs mooring stiffness S1 with a draft again of 0.55 m and Hmo 4.19 m. Further results are presented and extrapolated in Fig. 29.

Mooring forces increase linearly with the wave height. Higher forces are associated with S2 stiffer configuration, as expected. The average difference on front mooring forces between configurations S1 and S2 is 23.5%.

By lowering the structure and increasing the draft, there is a change on the mooring forces. This can be seen by comparing the curves S2 and S2Bs in Fig. 29. Indeed, by lowering the crest (i.e, increasing the draft) of 0.38 m (passing from dr1=0.55m to dr2=0.93 m) under configuration S2, we recorded a decrease on mooring forces of around 10% on the front line. This is also an expected result as forces on floating bodies, decreases when lowering the structure under mean water level where the amplitude of particles´ motion under wave action is smaller and decreases while increasing water depth.

The maximum F1/250 obtained on the rear mooring is for the S2 and draft of 0.55 m below sea water level, under Hm0=4.22 m. This force corresponds to F1/250=51.11 KN. Similar behavior of the front mooring is recognized for the rear mooring, despite performed tests failed to show results

as clearly as for the front mooring. Indeed, the size of the model and perhaps not enough difference on the two chosen stifnesses resulted in the over-looping of the curves representing the dependency of the rear mooring force on the significant wave height for S1 and S2 (Fig. 30). Nevertheless it is still clear that forces increase with the increasing wave height and that a lower structure (bigger draft) reduces the forces on the mooring line.

In average, the forces on the front mooring are twice as much the ones on the rear mooring that are therefore not negligible even if considerably smaller.

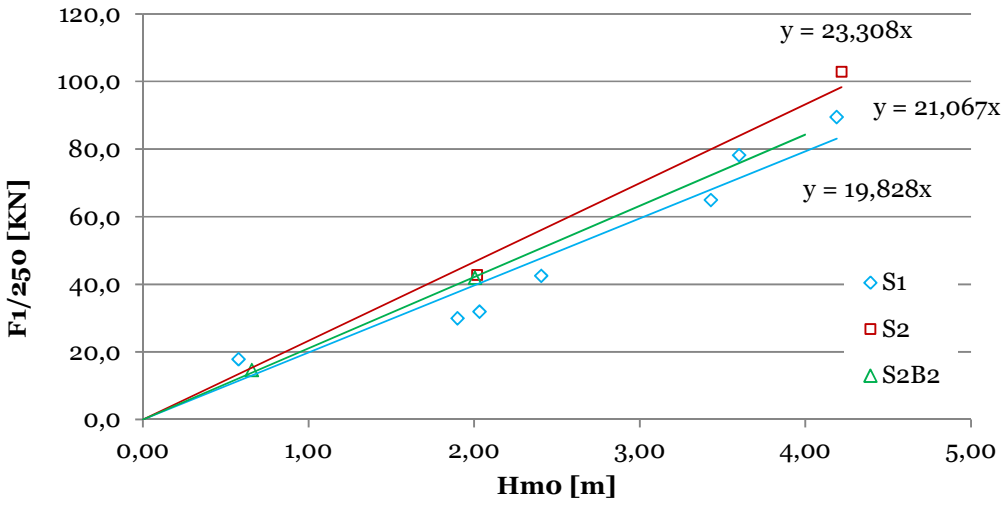


**Figure 29. Dependency of forces on FRONT mooring on Hmo, for S1 and S2 and S2B2. Full scale.**

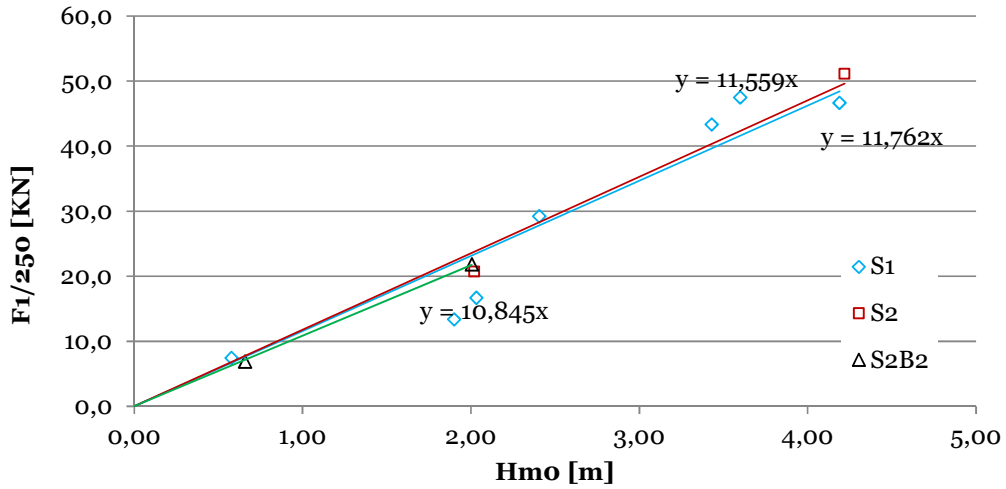


**Figure 30. Dependency of forces on REAR mooring on Hmo, for S1 and S2 and S2B2. Full scale.**

Finally, the minimum and maximum force distribution for the front line in test W4S2 has been plotted in exponential paper (Fig. 31). This shows a difference of around 40% between the two curves for expedience probabilities higher than 0.5%. Therefore, for bigger waves, it is expected the

mooring lines will have to work at far away from operating conditions and therefore need to be carefully designed.

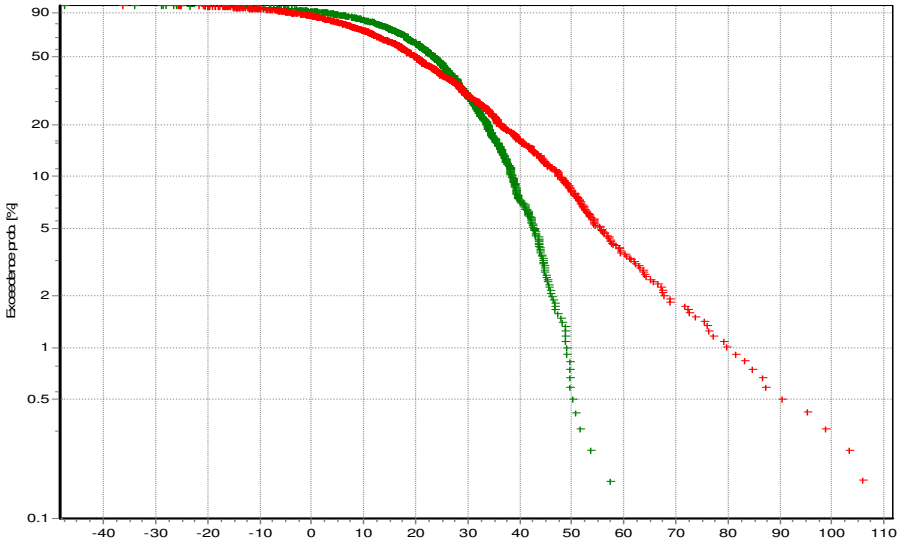


**Figure 31. Force distribution Min (green) and Max (red) in KN, front mooring, Hm0= 4.22 and S2.**

## *5.5 Overtopping and functioning of the pump system*

The measurement of the overtopping flows was not possible in the present setup because of physical restrictions. It would have been indeed impossible to set up the necessary measuring equipment maintaining the right weight/buoyancy of the structure. Nevertheless, it is believed the indications given in Chapter 2, taking into account the hypothesis, are accurate. A propeller was installed at the entrance of the pipe at approximately 0.06 m from the entrance (1.5 m real scale). From this point we have measurements of number of revolutions per second (RPS). The number of revolutions is directly proportional to the overtopping flow rate over the crest. Therefore conclusions are made based on this parameter.

No overtopping occurred for low sea states (W1 and W2) corresponding to Hm0=0.6 m real scale in the floating configuration for Rc1=0.7 m; indeed RPS is equal to zero. When using a lower crest level Rc2=0.32 m we can see some overtopping for W2 but still no overtopping for W1. This is to be attributed to the influence of the movements of the device riding the incoming weaves.

In our case, no significant difference among the three floating configurations has been found (S1, S2, S2B2), despite the stiffer mooring did prevent a bit the movements (Fig. 32).No significant difference for S1 and S2 and S2B2 is recorded, but it is unlikely that a situation with a stiffer mooring would result in a lower overtopping, keeping all the other conditions the same.

Instead, influence of the movements of the floating body on the overtopping can be better noticed when fixing the device (tests´tag: _Fixed_). It is clear that when the device is fixed instead of floating, bigger volumes of water enter then the reservoir. Indeed, overtopping does occur for W1 and W2 but most of all the overtopping increases of 38% for W3 and 53% for W2 when comparing the fixed configuration to the floating configuration with the same crest level (green and purple trend lines in Fig.32).

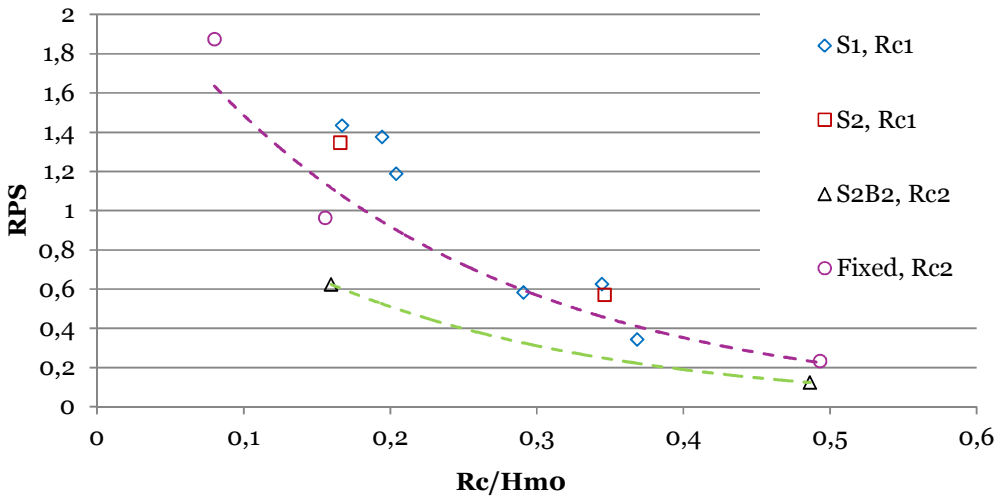


**Figure 32. Dependency of the RPS on Hmo for different configurations.**

From the recordings of the 2 small wave gauges inside the reservoir it emerged that the water did never spilled out of the reservoir, not even with higher wave conditions, testifying that the pump mechanism is working properly and pump capacity was sufficient to handle overtopping flow.

Standing waves across the reservoir have been noticed as a constant in all tests.

## *5.6 Motion transfer function*

The motion response of the structure is reported for surge, heave and pitch. We here compare the input (waves´ spectral density) to the response (movements´ spectral density) to obtain the motion transfer function as the ratio between these two. This is done for two different wave conditions in order to cover a wider range of frequencies. The selected wave conditions for this procedure are the ones obtained by the tests: W41S1Hs0.12Tp1.5 and W3S1D0605 (Fig. 33, 34 and 35, top).

For surge we can see a huge natural response (Fig. 33, middle). Indeed, while all the wave energy is concentrated around 0.6-0.9 Hz (Fig 33, top), the peak response is instead around 0.4-0.5 Hz. This is confirmed by the fact that the natural oscillation for surge was found to be 2.5 s, (frequency=1/T). The transfer function (Fig 33, bottom) for values lower than 0.6 Hz has not been reported as subject to height uncertainties. Indeed, being the transfer function the ratio between the response spectrum and the wave energy spectrum, the result features very high values being the energy input very small. Instead, it is clear that under the influence of waves, the motion is dominated by the moorings.

For heave, the natural response is concentrated ad very low frequencies (Fig. 34, middle). This is the case because the free oscillations have been found to have a very long period. A small response is also recorded under the action of the incoming waves, around 0.6 Hz close to the peak wave period. Also in this case, the transfer function is reliable only for values of Hz bigger than 0.4 (Fig. 34 bottom).

For pitch, we have a response that matches very well the energy input (Fig, 35, middle). Indeed the response is concentrated between 0.5 and 1.4 Hz. As for the previous two transfer functions, also here and for the same reasons, the reliable transfer function must be considered for Hz>0.5 (Fig 35, bottom).

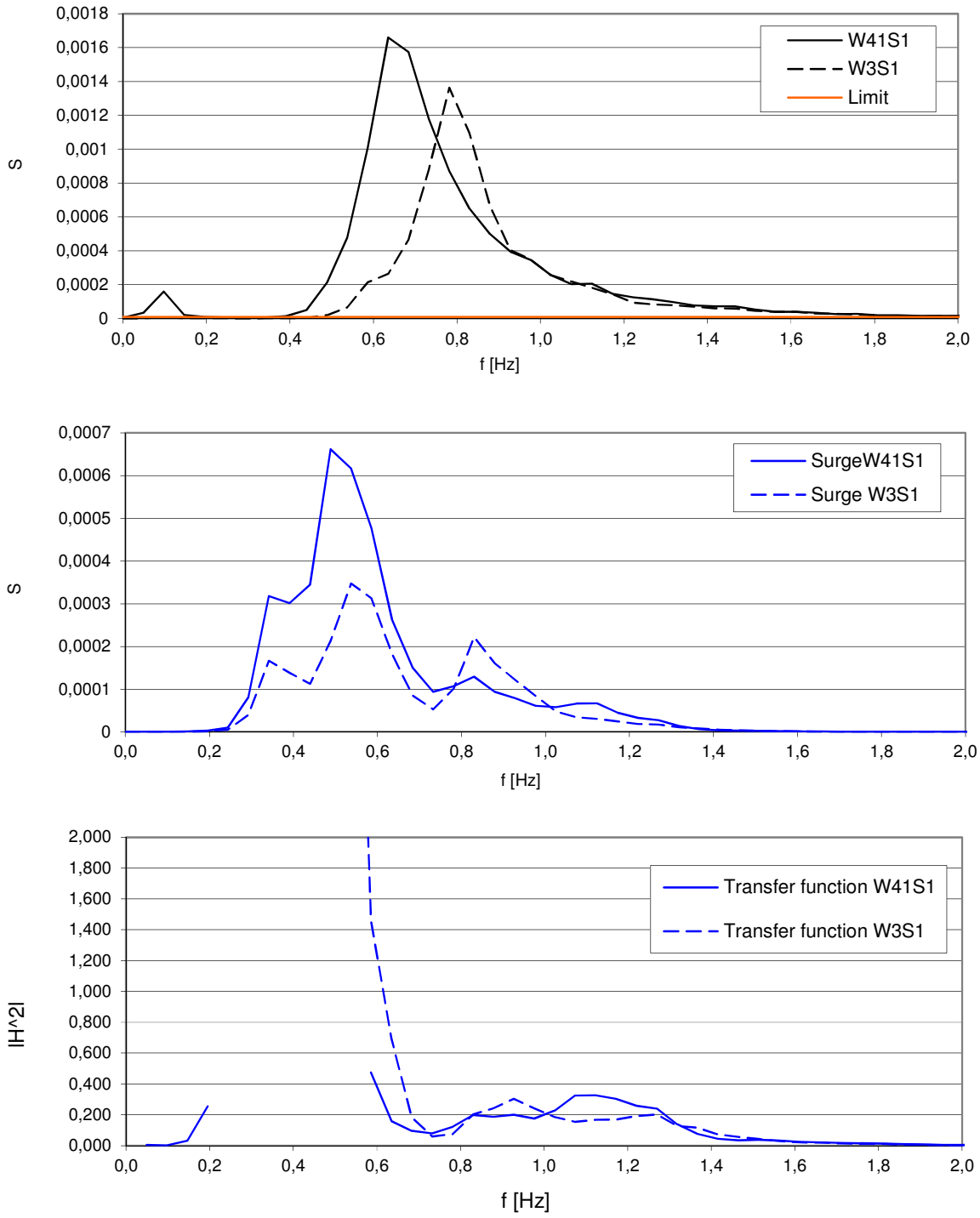


**Figure 33. Input, response and transfer function for Surge.**

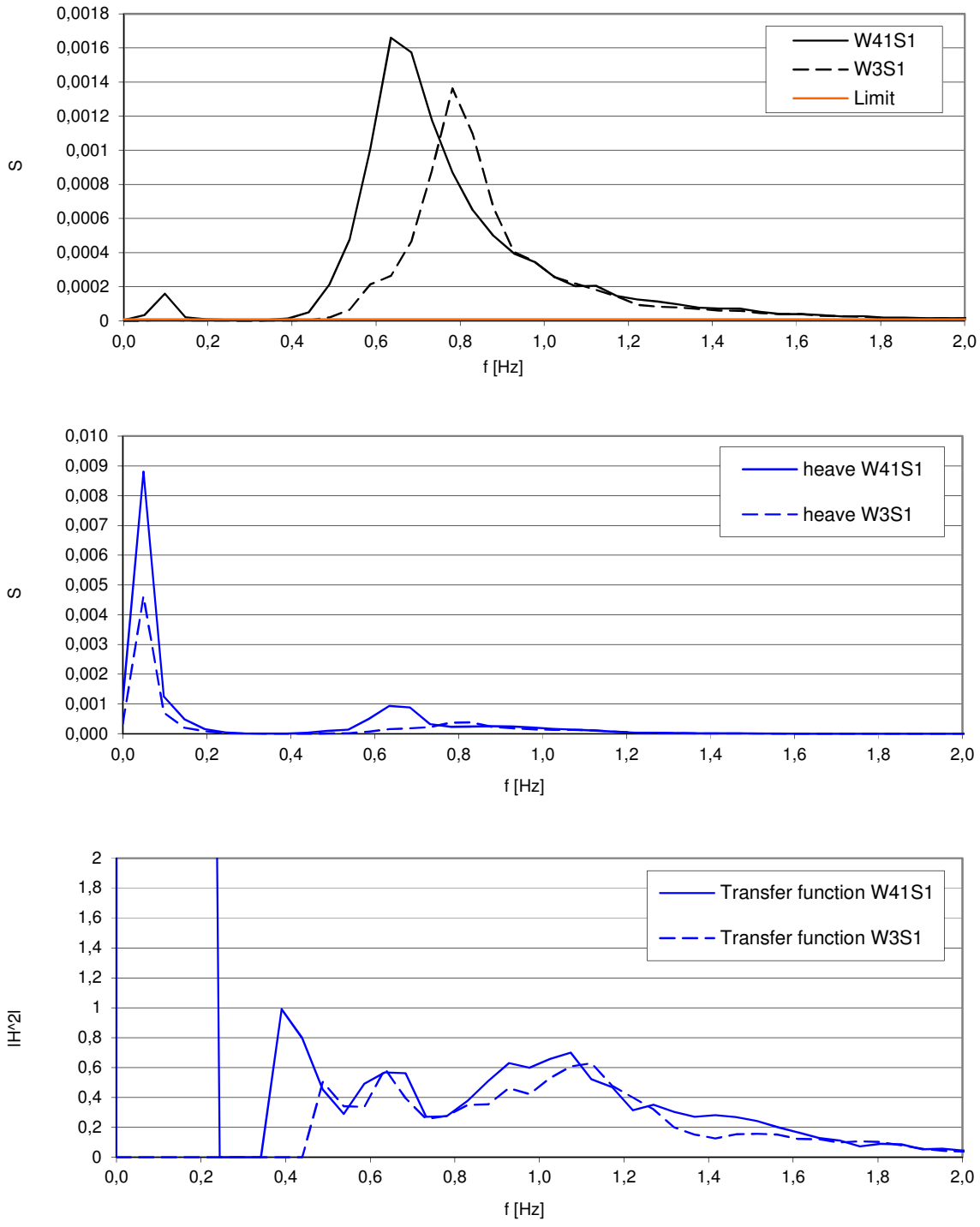


**Figure 34. Input, response and transfer function for Hevae.**

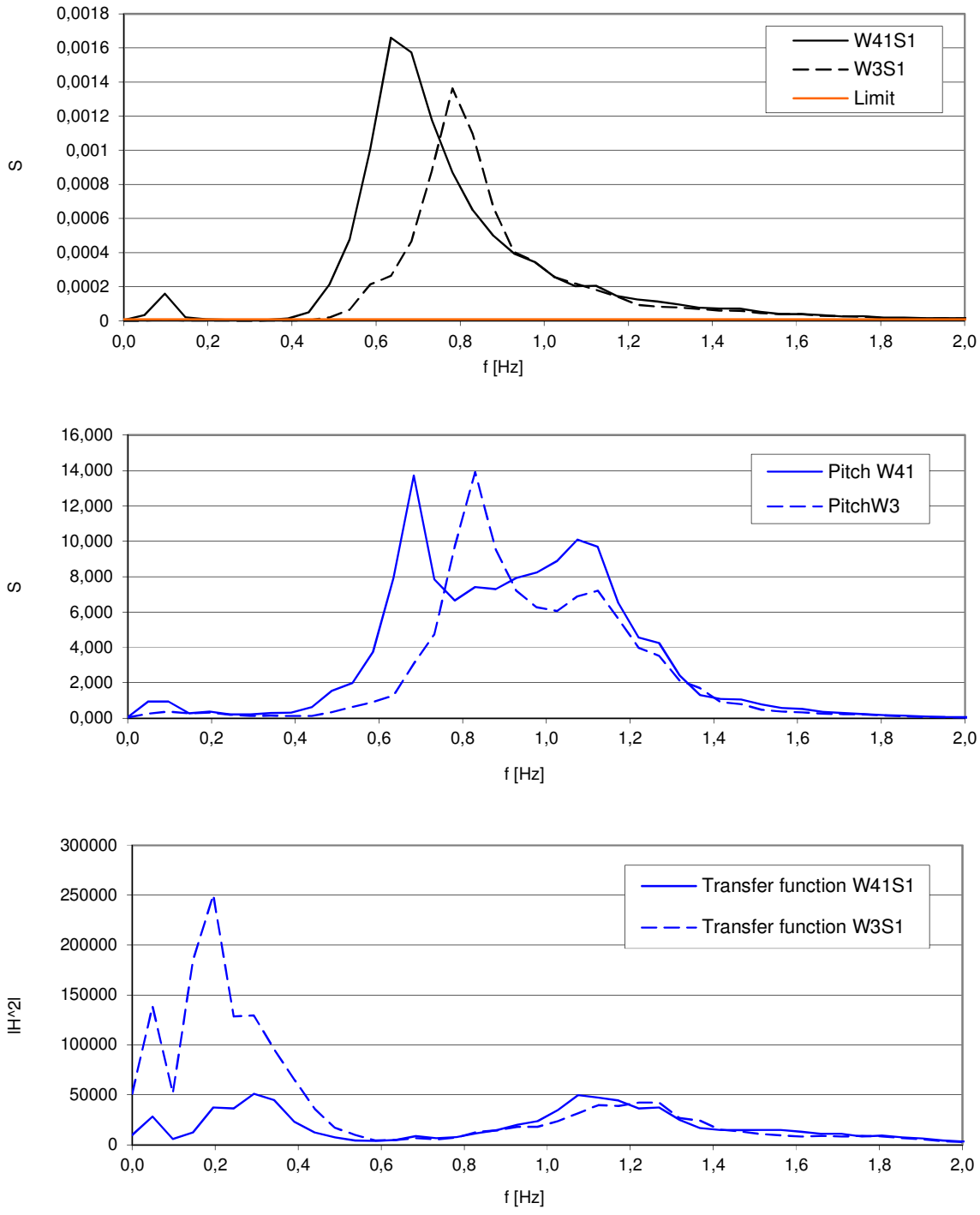


**Figure 35. Input, response and transfer function for Pitch.**

## *5.7 Conclusions*

A total of 18 tests have been run with WEBAP model in scale 1:25 in different configurations and wave conditions. Previously, free oscillation tests had showmen natural frequency for surge corresponding to 2.5 seconds. For heave 20 seconds and 2.8 seconds for pitch.

The maximum generated wave height corresponds to Hs=4.22 m and Tp=8.715 s. Under the action of these waves, the maximum mooring force occurred. This force is 102.9 KN on the front mooring and 51.11 KN on the rear mooring.

Higher forces correspond to bigger waves and stiffer moorings.

Forces on front mooring are in average twice bigger than forces on the rear mooring.

By lowering the structure, the forces on mooring are reduced. By passing from dr1=0.55 and dr2=0.93 it is expected a decrease of the mooring force of around 10%.

Movements of the floating body have a negative effect on the overtopping. No overtopping occurs for Hs=0.6 m and Hs=1.0 m for Rc1=0.70 m. The smallest overtopping event recorded was for Rc2=0.32 m, draft = 1.43 m and Hs=0.70 m. This situation generated RPS in average 10 times smaller than the tests with Hs~4m.

The influence of movements on the overtopping is increasing with Hs. For Hs=2.4 m the overtopping decreases of 38% compare to the case of a fix structure with same Rc, while decrease of 53 %for Hs=4.8 m.

Transfer functions for surge, heave and pitch have been given. It seems that the first two are dominated by the mooring characteristics. The heave movement is very slow. During the tests it was noticed that the device was riding the waves very much.

# 6 Notes and suggestions

Based on results it is clearly convenient to extend the front ramp in order to maximize the overtopping. Nevertheless the extension should be realized with a solid material in order to guarantee survivability and to avoid the energy of the incoming waves to be transferred behind the ramp instead of being utilized to maximize the overtopping. The improvements plotted in section 2.2 should be reduced if a flexible material is used instead.

The ramp inclination angle of 30˚is optimal for overtopping maximization. Bigger angles will prevent water from entering the reservoir, while smaller angles will induce some breaking. Nevertheless, overtopping varies only of few points percentage when angles vary between 23˚ and 35˚.

In the Baltic Sea, the gradient in water column density is bigger for water depths greater than 40 m. Moreover, losses for a long pipe extending from the sea surface to the sea bed can not be neglected. Indeed, in our case it resulted that a minimum head of 0.13 m is necessary to have the pump mechanism to start up, for a 70 m long pipe.

During the testing phase, it was clear by observation that the device was riding the waves very much. This has negative effect on the overtopping which is decreased proportionally to the amplitude of the incoming waves. It is suggested that ballast is added to have a lower crest obtaining at the same time lower forces on the mooring and increased overtopping.

From section 2.2 of the present report it is suggested that a WEBAP with the overall dimensions of 13.5 m length, Rc1=0.70m and draft =0.55+1.5=2.05 m (corresponding to one of the tested configurations, with ramp extension of 4 m) will generate an overtopping q=0.2 $m^3$/s for Hs=0.6 m and q=1.2 $m^3$/s for Hs=1.0 m. For the same geometry but with a crest level of Rc2=0.32 m and a draft of 0.93+1.5=1.43 m the calculated overtopping is q=0.75 $m^3$/s for Hs=0.6 m. This is contradicted by the laboratory tests where no overtopping occurs for those cases. This must be attributed not only to the fact that the ramp extension is flexible and therefore fails on its purpose of directly the water up to the ramp, but mainly to the movements of the device riding the waves.

Means for reducing movements must be applied.

## *Reference*

Goda, Y. (1985), Random Seas and Design of Maritime Structures, University of Tokyo Press, Tokyo, Japan.

McCutcheon, S.C., Martin, J.L, Barnwell, T.O. Jr. 1993. Water Quality in Maidment, D.R. (Editor). Handbood of Hydrology, McGraw-Hill, New York, NY (p. 11.3).

Kofoed J. P. (2002): “Wave Overtopping of Marine Structures –Utilization of Wave Energy”. Ph. D. Thesis, defended January 17, 2003 at Aalborg University. Hydraulics & Coastal Engineering Laboratory, Department of Civil Engineering, Aalborg University.

Van der Meer, J.W. and J. P. F. M. Janssen (1995): “wave run up and wave overtopping at dikes”. Technical report, Task Committee Reports, ASCE.

## *A - Appendix*

# MTi

MINIATURE ATTITUDE AND HEADING REFERENCE SYSTEM

xsens

The MTi is a miniature size and low weight 3DOF Attitude and Heading Reference System (AHRS).The MTi contains accelerometers, gyroscopes and magnetometers in 3D, and as such is an Inertial Measurement Unit (IMU) as well. Its internal low-power signal processor provides real-time and drift-free 3D orientation as well as calibrated 3D acceleration, 3D rate of turn and 3D earth-magnetic field data.

The MTi is an excellent measurement unit for stabilization and control of cameras, robots, vehicles and other (un)manned equipment.

## Highlights

- Real-time computed attitude/heading and inertial dynamic data
- 360° orientation referenced by gravity and earth magnetic field
- Integrated 3D gyroscopes, accelerometers and magnetometers
- On board DSP with realtime sensor fusion algorithm
- Gyroscopes enable high-frequency orientation tracking
- High update rate (256 Hz), inertial data at max 512 Hz
- Individually calibrated for temperature, 3D misalignment and sensor cross-sensitivity
- Accepts and generates synchronization pulses

## Compact Design

- Compact and robust design
- Easy integration in any system or application (OEM)
- Low weight, ultra-low power consumption

## High performance

The MTi uses gyroscopes, accelerometers and magnetometers in order to determine the orientation. The sophisticated Xsens sensor fusion algorithm copes with temporary magnetic disturbances and short-term accelerations, resulting in a reliable real-time orientation estimate. Additionally, the MTi SDK incorporates a magnetic field mapping routine to correct for hard and soft iron effects.

## Application-specific settings for optimal accuracy

As the MTi is used in a wide range of applications, the embedded sensor fusion filter algorithm should be adapted to the specific application to ensure the best achievable accuracy. Xsens has tested and tuned the sensor fusion filter settings for a range of common motion scenarios. The unique sets of parameters are provided in user-settable Scenarios. Using the correct scenario for your application ensures highest attainable accuracy for the application at hand, tested by Xsens, without the need for lengthy extensive tuning with uncertain results. Just set and go.

## Maximum flexibility

The MTi can be software or hardware synchronized (both SyncIn and SyncOut). The extensive SDK ensures full control of the MTi and makes interfacing to the MTi easy. The SDK provides interfaces at multiple levels: intuitive Windows GUI software, API binary libraries (Windows, Linux) as well as supplying source code implementing the MTi binary communication protocol for easy integration on any platform. With the MTi, your preferred solution is easy and fast to realize.

## Output

- 3D orientation (360°)
- 3D acceleration
- 3D rate of turn
- 3D magnetic field

## TYPICAL USAGE APPLICATIONS

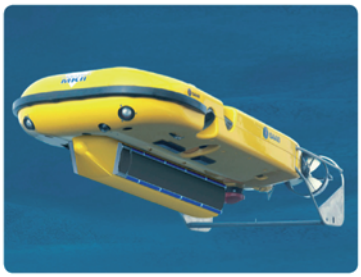

### Subsurface marine

- Control and stabilization of AUV/ROV/UUV
- Orientation correction for USBL systems

The MTi will fit even in the smallest AUV/ROV/UUV, because of its small footprint. Still, it offers a remarkable accuracy in terms of orientation, dynamic data and immunity to magnetic disturbances, it has proven to be an excellent choice for small to medium sized submersibles. The on-board digital processor outputs orientation for instantaneous attitude control. The MTi can be used as a stable compass as well, using various hard- and software features. Another good example of the application of the MTi is the orientation correction for USBL systems. The direct low-level communication allows full and easy control.

### Surface Marine

- State estimation of all kinds of ships and platforms
- Orientation correction for echo sounders and sonar
- Sensor input for Dynamic Positioning (DP) systems
- Correction of sensor systems on buoys

The MTi is used for state estimation on ships, ranging from small survey vessels to large container ships. The information can be stored or displayed real-time. The MTi easily fits in small systems, such as echo sounders, sonar heads and harbour protection systems. Because of small data- packages the MTi is extremely suitable for installation in buoys to monitor orientation for long-term measurements, where storage capacity may be an issue. The MTi is also used in research concerning sea and weather dynamics.

### Unmanned ground vehicles and robotics

- Autonomous attitude control of driving and walking robots
- Control and stabilization of Unmanned Ground Vehicles (UGV)

Using the MTi in robotics is a logical choice when accurate attitude and a direct communication is mandatory. The MTi is valued for its low size and weight and can be easily configured in accordance with the user's requirements. In walking, humanoid and biped robots, the low response time of the MTi proves to be essential to provide reliable balance control. For unmanned ground vehicles, the MTi is just as useful, providing orientation and dynamic information at a very low cost. The MTi has been used by teams in all DARPA Challenges.

### Other

- Camera/antenna stabilization
- Vehicle dynamics
- Bore technology

The MTi's internal sensors provide full 3D dynamics data (acceleration and rate of turn) of any vehicle. The small size allows the MTi to be used in small-diameter pipes (under 40 mm). Together with odometry, the MTi can serve as an input to provide a full map of underground piping. The MTi can be used in many other miscellaneous applications, such as camera stabilization and antenna aiming.

## ACCESSORIES

### Cable options

**CA-USB2**

USB cable

**CA-SERi**

Serial cable
RS232 + pigtail

**CA-DB9i**

RS232, DB9
power

**PA-MP**

Power adapter
(for CA-DB9i only)

## MTi DEVELOPMENT KIT

### MTi Development Kit (MTi DK)

The MTi DK contains the following:

- MTi (any configuration)
- USB cabling
- MT Software Development Kit (see below)
- Hardcopy documentation
- Optional: serial cabling
- Suitcase

### MT Software Development Kit (MT SDK)

The MT SDK is an extensive set of tools for every level of interfacing, which allows configuring the MTi to the user needs, reading out and storing data and (re-)processing MTi data previously recorded. It also allows the user to generate own source code using commands and code examples provided.


### The MT SDK contains:

**MT Manager**
An easy-to-use graphical user interface with possibilities to configure Xsens' sensors, read out, store and show data in real-time charts and visualizations.

**MT COM-object API and DLL API for Windows**
Integrating the MTi in Windows programs, such as Matlab, C++ and Excel is made easy with the MT COM-object API and the DLL API. User-modifiable example code for Matlab, C++ and Excel (VBA) is included.

**C++ Class and binary communication for any (RT)OS**
A C++ class is available for users who want to use the MTi on a binary level. Direct communication without using the C++ class is possible, following the fully documented communication protocol.

**Magnetic Field Mapper plug-in**
The Magnetic Field Mapper plug-in enables compensation for hard and soft iron effects.

xsens

## MTi TECHNICAL SPECIFICATIONS

### Attitude and Heading

| | |
|---|---|
| Static accuracy (roll/pitch) | <0.5 deg |
| Static accuracy (heading)[1] | <1 deg |
| Dynamic accuracy[2] | 2 deg RMS |
| Angular resolution[3] | 0.05 deg |
| Dynamic range: | |
| - Pitch | ± 90 deg |
| - Roll/Heading | ± 180 deg |
| Maximum update rate: | |
| - Onboard processing | 256 Hz |
| - External processing | 512 Hz |
| Specified performance operating range[4] | 0...+55 °C |

### Interfacing

| | |
|---|---|
| Digital interface | RS-232, RS-485, RS-422 (max 921k6 bps) and USB (ext. converter) |
| Operating voltage | 4,5 - 30V |
| Power consumption | 350 mW |
| Interface options I/O | SyncOut, AnalogIn, SyncIn (depends on digital interface) |

### Maximum operational limits

| | |
|---|---|
| Ambient temperature operating range[4] | -40...+85 °C |

## INDIVIDUAL SENSOR SPECIFICATIONS

| Sensor performance | Rate of turn | Acceleration | Magnetic field |
|---|---|---|---|
| Dimensions | 3 axes | 3 axes | 3 axes |
| Full Scale (standard) | ± 300 deg/s | ± 50 m/s² | ± 750 mGauss |
| Linearity | 0.1% of FS | 0.2% of FS | 0.2% of FS |
| Bias stability[5] | 1 deg/s | 0.02 m/s² | 0.1 mGauss |
| Scale Factor stability[5] | - | 0.03% | 0.5% |
| Noise | 0.05 deg/s/√Hz | 0.002 m/s²/√Hz | 0.5 mGauss |
| Alignment error | 0.1 deg | 0.1 deg | 0.1 deg |
| Bandwidth | 40 Hz | 30 Hz | 10 Hz |
| Max update rate | 512 Hz | 512 Hz | 512 Hz |

## HARDWARE SPECIFICATIONS

### Housing

| | |
|---|---|
| Dimensions (WxLxH) | 58x58x22 mm |
| Weight | 50 g |

### Options

| Interface: | | Full scale acceleration: | | Full scale rate of turn: | |
|---|---|---|---|---|---|
| RS-232 | 28 | | | 150 deg/s | G15 |
| RS-485 | 48 | 5g (50 m/s²) | A53 | 300 deg/s | G35 |
| RS-422 | 68 | 18g (180 m/s²) | A83 | 1200 deg/s | G25 |

| | |
|---|---|
| Product code: | MTi-## A## G## |
| Standard version: | MTi-28 A53 G35 |

The MTi is RoHS compliant

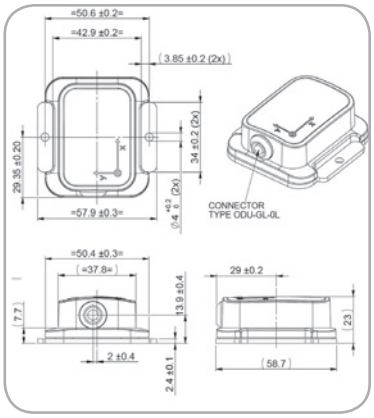


Note: Specifications subject to change without notice

1. in homogeneous magnetic environment
2. under condition of a stabilized Xsens sensor fusion algorithm
3. 1 standard deviation of zero-mean angular random walk
4. non-condensing environment
5. deviation over operating temperature range 1σ

xsens

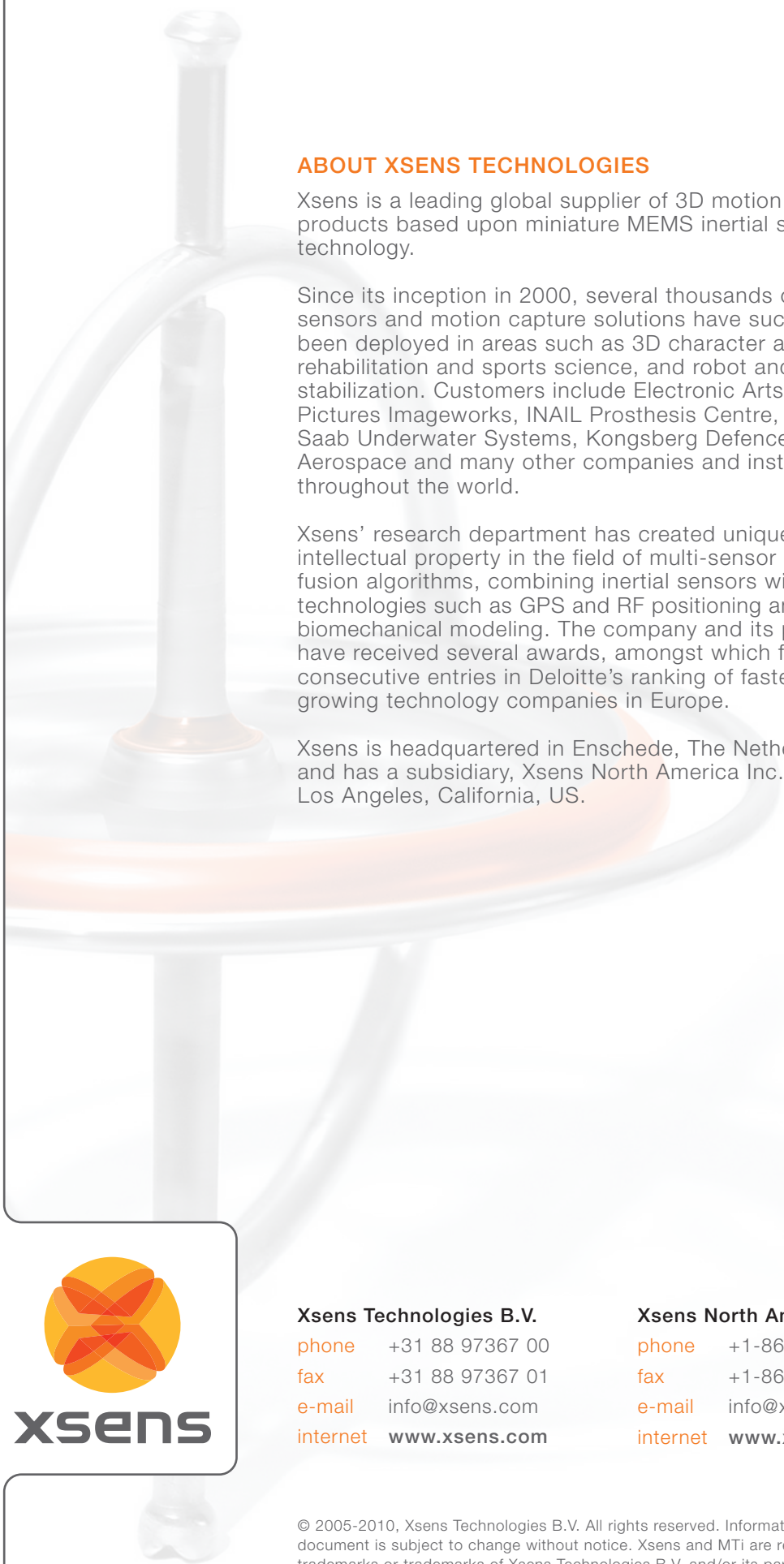

## ABOUT XSENS TECHNOLOGIES

Xsens is a leading global supplier of 3D motion tracking products based upon miniature MEMS inertial sensor technology.

Since its inception in 2000, several thousands of motion sensors and motion capture solutions have successfully been deployed in areas such as 3D character animation, rehabilitation and sports science, and robot and camera stabilization. Customers include Electronic Arts, Sony Pictures Imageworks, INAIL Prosthesis Centre, Daimler, Saab Underwater Systems, Kongsberg Defence & Aerospace and many other companies and institutes throughout the world.

Xsens' research department has created unique intellectual property in the field of multi-sensor data fusion algorithms, combining inertial sensors with aiding technologies such as GPS and RF positioning and biomechanical modeling. The company and its products have received several awards, amongst which four consecutive entries in Deloitte's ranking of fastest growing technology companies in Europe.

Xsens is headquartered in Enschede, The Netherlands and has a subsidiary, Xsens North America Inc. in Los Angeles, California, US.

xsens


**Xsens Technologies B.V.**

phone +31 88 97367 00
fax +31 88 97367 01
e-mail info@xsens.com
internet **www.xsens.com**

**Xsens North America Inc.**

phone +1-866-973-6787 (toll-free)
fax +1-866-973-6701
e-mail info@xsens.com
internet **www.xsens.com**